OXYGEN UPTAKE AND VERTICAL TRANSPORT DURING DEEP CONVECTION EVENTS IN THE LABRADOR SEA AND ITS INTERANNUAL VARIABILITY

A Dissertation
Presented to
The Academic Faculty

By

Daoxun Sun

In Partial Fulfillment
of the Requirements for the Degree
Doctor of Philosophy in the
School of Earth and Atmospheric Sciences

Georgia Institute of Technology

May 2020

OXYGEN UPTAKE AND VERTICAL TRANSPORT DURING DEEP CONVECTION EVENTS IN THE LABRADOR SEA AND ITS INTERANNUAL VARIABILITY

Approved by:

Dr. Takamitsu Ito, Advisor
School of Earth and Atmospheric Sciences
Georgia Institute of Technology

Dr. Annalisa Bracco, Advisor
School of Earth and Atmospheric Sciences
Georgia Institute of Technology

Dr. Emanuele Di Lorenzo
School of Earth and Atmospheric Sciences
Georgia Institute of Technology

Dr. Jie He
School of Earth and Atmospheric Sciences
Georgia Institute of Technology

Dr. Curtis Deutsch
School of Oceanography
University of Washington

Date Approved: March 11, 2020

ACKNOWLEDGEMENTS

First and foremost, my deepest gratitude goes to my advisors, Dr. Takamitsu Ito and Dr. Annalisa Bracco, for their continuous encouragement and guidance throughout my graduate studies. I feel very lucky to have two great advisors with different styles. I really enjoyed working with both of them and learnt a lot. I also wish to thank my committee members, Dr. Emanuele Di Lorenzo, Dr. Jie He and Dr. Curtis Deutsch for their time and support. It is a great honor for me to have the insights from the best experts in our fields.

It has been a great pleasure to work with all the colleagues and friends in the School of Earth and Atmospheric Sciences at Georgia Institute of Technology. They are warm-hearted and always willing to help when needed. I appreciate all the inputs from them for my researches and this dissertation.

Last my thanks would go to my beloved family for their loving considerations and great confidence in me all through these years. Especially, I would like to thank my wife, a super lady who brings my little princess into the world and keeps this little troublemaker away from me when I need to focus. She makes it possible to finish this dissertation.

TABLE OF CONTENTS

LIST OF TABLES

LIST OF FIGURES

SUMMARY

Dissolved oxygen (DO) is essential for marine life and biogeochemical cycling. To a first order approximation, DO is determined by the competition between ocean ventilation and biological productivity. Approximately 21% of the atmospheric gases is oxygen, and the waters at the ocean surface are enriched in oxygen. Ventilation occurs through a suite of physical processes that brings the DO-rich surface waters into the interior ocean. This dissertation combines two works that closely examine the ventilation of oxygen in the region of deep water formation, and explore the relationship between air-sea oxygen flux and surface forcing aiming at deepening our understanding of the processes that regulate he DO inventory. Through these analyses we develop a framework to understand the oxygen to ocean heat content (O_2-OHC) ratio in the ocean interior. Both works focus on the Labrador Sea and include a theoretical development and its validation using a suite of numerical sensitivity experiments.

The first work leads to two main conclusions. 1) Both the duration and the intensity of the winter-time cooling are important to the total O_2 uptake for a convective event. Stronger cooling leads to deeper convection and brings oxygen into deeper depths. Longer duration of the cooling period increases the total amount of oxygen uptake over the convective season. 2) The bubble-mediated influx of oxygen can increase oxygen uptake, but part of the contribution is compensated by the weakening the diffusive influx because the air-sea disequilibrium of oxygen is shifted towards supersaturation. The degree of compensation between the diffusive and bubble-mediated gas exchange depends on the relative strength of oceanic vertical mixing and the gas transfer velocity. Strong convective mixing reduces the degree of compensation so that the two components of gas exchange together drive exceptionally strong oceanic oxygen uptake. A numerical model with idealized domain and non-hydrostatic dynamics is used to test the hypotheses in this work.

The second work explores what controls the O_2-OHC ratio during deep convection.

Models of different complexities ranging from 1-D convective adjustment model to a regional ocean circulation model that includes a complex biogeochemical module are used. The bubble injection increases the oxygen flux and the magnitude of the O_2-OHC ratio under intense convective events. Longer cooling duration leads to a larger magnitude of the O_2-OHC ratio. The pre-conditioning of the vertical gradients in oxygen and temperature are important for the O_2-OHC ratio under different climate scenarios.

With these two works, we highlight a few key mechanisms that are important to regulate the DO inventory in the ocean interior, but further efforts are needed to understand the global DO variability and to constrain the deoxygenation potential under a warming climate.

CHAPTER 1
INTRODUCTION AND BACKGROUND

1.1 Dissolved Oxygen in the Ocean

The concentrations of dissolved oxygen (DO) is essential to many aspects of marine chemistry and ecosystem dynamics (*Keeling et al.*, 2010). DO is directly related to the biogeochemical cycling of carbon, nitrogen, phosphorus and trace elements in the ocean (*Schlesinger and Bernhardt*, 2013). Changes in DO levels directly influence most marine animals especially in regions with low DO concentration (*Vaquer-Sunyer and Duarte*, 2008). In a steady state, oxygen is consumed in the interior ocean due to the respiration of organic matter, which must be replenished by the newly ventilated surface waters. Given the estimate for the global export production of 5-13 PgC/year (*Laws et al.*, 2000; *Siegel et al.*, 2014; *Schlitzer*, 2000b), current oceanic oxygen inventory will be completely consumed within a few centuries without the continuing physical supply. DO in the ocean interior can be used as a tracer reflecting the ocean circulation and biological production (*Talley*, 2011). DO concentration is typically high near the regions of water mass formation, and decreases whenever the water is isolated from the surface (Figure 1.1). Giving this perspective, depletion of oxygen relative to saturation can be used as a measure of respiration in the interior ocean. Apparent Oxygen Utilization (AOU) (*Redfield*, 1958; *Broecker and Peng*, 1982) is one of the most widely used metrics, and is defined as

$$AOU = O_{2,sat} - O_2, \tag{1.1}$$

where $O_{2,sat}$ is the DO concentration at saturation and O_2 is the observed DO concentration. $O_{2,sat}$ is calculated from the potential temperature (T) and salinity (S). AOU can only represent the cumulative effect of respiration accurately when the surface water is

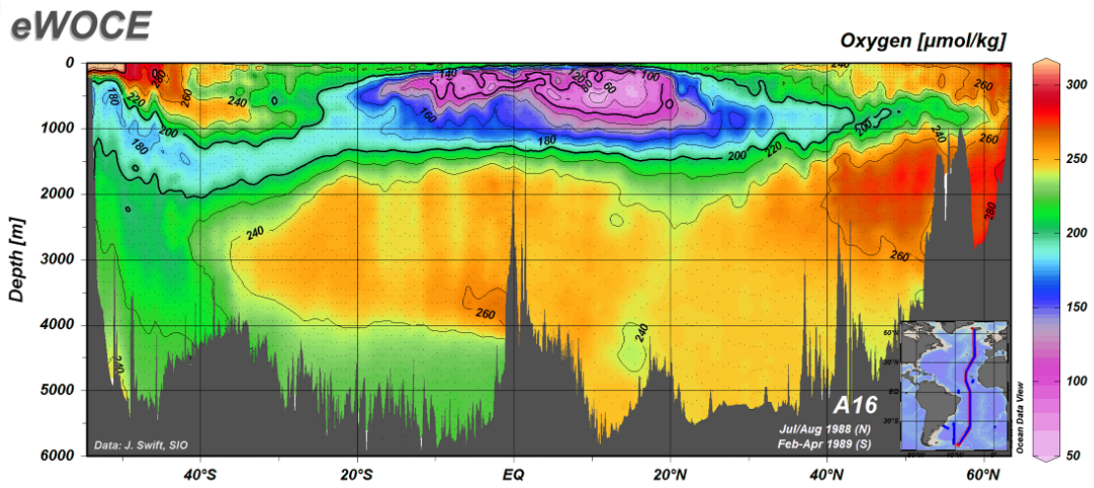

Figure 1.1: DO concentration along the World Ocean Circulation Experiment (WOCE) Line A16 from eWOCE Gallery (*Schlitzer*, 2000a).

fully equilibrated with the overlying atmosphere. This assumption is valid in many ocean regions because air-sea equilibration of oxygen is generally rapid relative to ocean circulation timescales (*Broecker and Peng*, 1982; *Williams and Follows*, 2011). However, the surface water could be undersaturated in regions where deep convection occurs as shown by *Ito et al.* (2004) using a numerical model. Undersaturation at the polar outcrop can significantly impact the oceanic oxygen inventory because the oxygen supply to the deep waters occurs only through subduction and deep convection. These events occur only during the cold season in the high latitude oceans. Therefore, studying the oxygen uptake during deep convection events is fundamental to investigate the inventory and distribution of oxygen and the related biogeochemical processes.

1.2 Surface oxygen flux

Studies about noble gases suggest that both diffusive and bubble-mediated mechanisms are important for air-sea gas exchange (e.g. *Hamme and Emerson*, 2002; *Hamme and Severinghaus*, 2007). In numberical simulations, the diffusive gas exchange term usually represents the molecular diffusion and the subsequent turbulent transfer, which is driven by the concentration gradient between the water at the ocean surface and the atmosphere. The

efficiency of gas transfer depends on the molecular diffusivity of the gas and the turbulence field at the interface. It is usually represented as

$$F_{dif} = G(\frac{p_{atm}}{p_0}c_{sat} - c), \tag{1.2}$$

where G is the gas transfer velocity, p_{atm} is the atmospheric pressure, p_0 is the standard atmospheric pressure, c_{sat} is the saturated concentration of selected gas at standard atmospheric pressure, which is a function of temperature and salinity, and c is the actual surface concentration. G is usually further parameterized as a function of wind speed, sea ice coverage and Schmidt number of the gas (*Wanninkhof*, 1992; *Nightingale et al.*, 2000; *Ho et al.*, 2006). A common form of the parameterization of the gas transfer velocity in models is (e.g. *Ito et al.*, 2011)

$$G = \alpha(1 - f_{ice})(\frac{u_{10}}{U_0})^2(\frac{Sc}{660})^{-0.5}, \tag{1.3}$$

where f_{ice} is the ice coverage at the ocean surface, α is the closure coefficient, u_{10} is the 10 m wind speed, U_0 is the reference wind speed, and Sc is the Schmidt number.

When surface waves break, air bubbles may form and be pushed into the surface water, which intensifies the air-sea gas exchange (*Monahan and Torgersen*, 1990; *Asher and Wanninkhof*, 1998; *Hamme and Severinghaus*, 2007). Relatively small bubbles can completely collapse and inject the air into the surface water, which is usually named as injection mechanism, while large bubbles may enhance diffusive gas exchange through increased pressure when the bubble is pushed underneath the water surface, which is often referred as the exchange mechanism (*Fuchs et al.*, 1987; *Merlivat and Memery*, 1983; *Woolf and Thorpe*, 1991; *Keeling*, 1993; *Hamme and Emerson*, 2002, 2006). The total bubble-mediated gas exchange can be written as (*Hamme and Emerson*, 2006)

$$F_{bub} = (V_{inj} + V_{ex}D_c^x\alpha_C^y)\chi_C, \tag{1.4}$$

where V_{inj} and V_{ex} are the fluxes due to injection and exchange, respectively, and χ_C is the atmospheric mole fraction of gas C. The exchange mechanism depends on the diffusion coefficient D_C and the Bunsen solubility coefficient α_C, but the power-law dependence is still unclear. Different power-law exponents, x and y, have been suggested by different studies (*Keeling*, 1993; *Jenkins*, 1988; *Hamme and Emerson*, 2002). *Hamme and Emerson* (2006) suggests that the flux from the injection mechanism is greater than or equal to that from the exchange mechanism for oxygen flux, with a ratio in the range of 1-2. The bubble-mediated fluxes are also correlated to surface wind, and are commonly modeled as proportional to wind speed cubed because whitecaps scales approximately with the cube of wind speed at the sea surface (*Hamme and Emerson*, 2006; *Asher and Wanninkhof*, 1998; *Monahan*, 1993). The bubble-mediated fluxes can cause the gases to be supersaturated at the ocean surface (*Fuchs et al.*, 1987; *Jenkins*, 1988; *Woolf and Thorpe*, 1991). At the sites of water mass formation, the bubble-mediated fluxes can increase gas uptake, and the increment for low solubility gases is more significant and can alter the composition of different gases in the ocean interior (*Hamme and Severinghaus*, 2007). For oxygen, accounting for the bubble-mediated fluxes is important for determining the biological productivity in the surface mixed layer since both processes can lead to oxygen supersaturation (*Hamme and Emerson*, 2006). As significant disequilibrium of oxygen can be observed at the sites of deep water formation (*Ito et al.*, 2004), including the bubble-mediated flux is potentially important to correctly simulate oxygen in ocean models (*Atamanchuk et al.*, 2020).

1.3 Deoxygenation under climate change

Both projections by Earth System Models (ESMs) and observational evidences indicate that DO in the ocean is decreasing, which is termed as ocean deoxygenation (*Bopp et al.*, 2002; *Matear et al.*, 2000; *Plattner et al.*, 2002; *Keeling et al.*, 2010; *Schmidtko et al.*, 2017). Observational estimates suggest that 1-2% of the global oxygen inventory has been lost in the last five decades (e.g. *Laffoley and Baxter*, 2019; *Manning and Keel-*

ing, 2006; *Schmidtko et al.*, 2017). The rate of decline differs among basins, and the most significant deoxygenation occurred in the North Pacific and tropical oceans (*Keeling et al.*, 2010), as water volumes with low DO concentration expanded and the new regions of hypoxia emerged (*Keeling et al.*, 2010; *Laffoley and Baxter*, 2019). Observational estimate by *Schmidtko et al.* (2017) indicate that the volume of waters with anoxic conditions has more than quadrupled since 1960. Earth System Models project the reductions in global oxygen inventory between 1-7% in the next century (*Keeling et al.*, 2010). Global warming is expected to reduce the oceanic oxygen content through two effects: directly, as the increased temperatures decrease oxygen solubility; and indirectly, as upper ocean warming induces increased stratification and reduced ventilation (*Keeling et al.*, 2010; *Laffoley and Baxter*, 2019). The upwelling of nutrient from deep ocean will also decrease when stratification strengthens, which may potentially increase the subsurface DO by reducing the export production of organic matter. However, the overall effect of stronger stratification is to decrease the global oceanic DO (*Bopp et al.*, 2013).

As the deoxygenation appears to be closely linked to the warming, estimation of the oxygen to ocean heat content (O_2-OHC) ratio can provide a useful constraint on the future deoxygenation. *Keeling and Garcia* (2002) used regional observations to bound the O_2-OHC ratio in a wide range from -2 to -10 $nmolO_2\,J^{-1}$, with larger ratios typically found at higher latitudes and over longer time scales. *Ito et al.* (2017) suggested that the O_2-OHC ratio of the upper ocean (0-1000 m) is -8.2 $\pm$ 0.66 $nmolO_2\,J^{-1}$ using objectively mapped historic O_2 data from 1958 to 2015. Earth System Models (ESMs) predict that the O_2-OHC ratio at the end of this century will be between -5.9 and -6.7 $nmolO_2\,J^{-1}$ (*Keeling et al.*, 2010). For the surface layers, the O_2-OHC ratio follows closely the dependency of solubility on temperature change, but when deeper layers are included, the ratio is much larger than what can be explained by the solubility change.

1.4 Deep convection in the Labrador Sea

The Labrador Sea is located between Greenland and Canada in the northwest North Atlantic. It is one of the few regions where deep convection occurs. The intense air-sea interaction drives the convective mixing (*Marshall and Schott*, 1999; *Pickart et al.*, 2002) and the sites of deep convection act as windows through which atmospheric gases enter into the deep waters (*Körtzinger et al.*, 2004). Deep convection mixes the surface waters to depths exceeding 2,000m and form a dense water mass, the Labrador Sea Water (LSW), that spreads across the northwest Atlantic between 1000 and 2200m (*Talley and McCartney*, 1982), carrying newly ventilated gas tracers along with it. The horizontal maps of a transient tracer (CFCs) have shown the spreading of the newly ventilated LSW into the North Atlantic (*Hall et al.*, 2007). The thick layer of LSW is well oxygenated ($\sim$290μM) implying the mixing of atmospheric oxygen during episodes of deep convection. The oxygen concentration of the newly formed LSW is an important component determining our ability to estimate the cumulative biological oxygen consumption using AOU. Historic observations show strong variance of oxygen on interannual to decadal timescales (*Falina et al.*, 2007; *van Aken et al.*, 2011). Many researches have been trying to address the major processes responsible for this variability, exploring, for example, the role of air-sea fluxes (*Luo et al.*, 2014), eddies (*Bracco and Pedlosky*, 2003; *Katsman et al.*, 2004) and fresh water fluxes (*Luo et al.*, 2016).

1.5 Objectives of this dissertation

Here two works aiming at understanding the oxygen uptake at sites of water mass formation are presented. Using the winter convective events in the Labrador Sea as example, we closely examine the oxygen uptake during convective events, and explore the relationship between oxygen flux and surface cooling through theoretical derivations and model simulations of various complexity. Better understanding the mechanisms controlling the

DO content of the newly formed deep water can provide insights into the variability of the oceanic DO content, and hopefully improve our ability to constrain future deoxygenation.

Chapter 2 illustrates the importance of bubble injection under different cooling scenarios through a quisi-equilibrium theory and numerical simulations using a non-hydrastatic model. Chapter 3 further explores the key factors that determine the O_2-OHC ratio during deep convective events using theoretical reasoning and numerical models of various complexity, from idealized to realistic. Chapter 4 summarizes our findings and proposes future work.

CHAPTER 2

OCEANIC UPTAKE OF OXYGEN DURING DEEP CONVECTION EVENTS THROUGH DIFFUSIVE AND BUBBLE MEDIATED GAS EXCHANGE

Published as

[1] Sun, D., T. Ito, and A. Bracco (2017), Oceanic uptake of oxygen during deep convection events through diffusive and bubble-mediated gas exchange. *Global Biogeochemical Cycles*, 31, 1579–1591.

Abstract

The concentration of dissolved oxygen (O_2) plays fundamental roles in diverse chemical and biological processes throughout the oceans. The balance between the physical supply and the biological consumption controls the O_2 level of the interior ocean, and the O_2 supply to the deep waters can only occur through deep convection in the polar oceans. We develop a theoretical framework describing the oceanic O_2 uptake during open-ocean deep convection events and test it against a suite of numerical sensitivity experiments. Our framework allows for two predictions, confirmed by the numerical simulations. First, both the duration and the intensity of the winter-time cooling contribute to the total O_2 uptake for a given buoyancy loss. Stronger cooling leads to deeper convection and the oxygenation can reach down to deeper depths. Longer duration of the cooling period increases the total amount of O_2 uptake over the convective season. Second, the bubble-mediated influx of O_2 tends to weaken the diffusive influx by shifting the air-sea disequilibrium of O_2 towards supersaturation. The degree of compensation between the diffusive and bubble-mediated gas exchange depends on the dimensionless number measuring the relative strength of oceanic vertical mixing and the gas transfer velocity. Strong convective mixing, which may occur under strong cooling, reduces the degree of compensation so that the two components of gas exchange together drive exceptionally strong oceanic O_2 uptake.

2.1 Introduction

The concentrations of O_2 have far reaching influence on the chemistry and biology of the global oceans. O_2 levels below 60μM, termed hypoxic conditions, are lethal for more than 50% of bottom dwelling organisms. More than 90% of organisms are impacted if the O_2 levels drop below 10 μM (*Vaquer-Sunyer and Duarte*, 2008). As the ocean absorbs heat in the warming climate, O_2 concentrations are expected to decrease due to a thermally-induced reduction of gas solubility and increasing ocean stratification that may inhibit convective mixing of O_2-rich surface waters into the deeper ocean (*Keeling et al.*, 2010). The latter effect can be particularly important for the oxygenation of the deep waters due to the dominant role of stratification in polar convection.

At a steady state, the O_2 inventory below the winter mixed layer must be sustained by the balance between physical O_2 supply and biological O_2 loss. Considering that the global export production is in the range of 6-11 PgC year^{-1} according to model and satellite estimates (*Laws et al.*, 2000; *Siegel et al.*, 2014; *Schlitzer*, 2000b) and that the global oceanic oxygen inventory is on the order of 2×10^{17} mol O_2 (*Garcia et al.*, 2010; *Boyer et al.*, 2013), the mean residence time (MRT) of deep O_2 (here deep refers to waters below the surface mixed layer, taken to be about 100 m) is less than two centuries, comparable to the timescales of the anthropogenic greenhouse forcing. Thus it is crucial to understand how O_2 is physically supplied to the deep ocean and how it might respond to climate variations.

The oxygen supply to the deep waters occurs, by and large, through high latitude subduction and deep convection during the cold season. Sites where deep convection occurs act as windows through which atmospheric gases enter into the deep waters (*Körtzinger et al.*, 2004). One such a region is the Labrador Sea, where the intense air-sea interaction in winter drives convective mixing (*Marshall and Schott*, 1999; *Pickart et al.*, 2002) from the surface to depths at times exceeding 2,000 m (*Lazier*, 1980; *Clarke and Gascard*, 1983; *Gascard and Clarke*, 1983; *Lazier et al.*, 2002; *Yashayaev et al.*, 2007; *Yashayaev*,

2007). The resulting dense water mass, the Labrador Sea Water (LSW), is well oxygenated ($\sim$290μM) implying the uptake and mixing of atmospheric oxygen, and spreads across the northwest Atlantic between 1000 and 2200 m (*Talley and McCartney*, 1982) carrying newly ventilated gas tracers along its path as shown by horizontal maps of a transient tracer (CFC) (*Hall et al.*, 2007).

The intense air-sea interaction also drives the strong flux of O_2 over the convecting ocean. The diffusive flux of oxygen into the ocean is driven by the concentration gradient between the sea surface and the overlying atmosphere, and its efficiency is controlled by the turbulence field at the air-sea interface. The magnitude of the diffusive flux is typically parameterized as the product of the gas exchange coefficient and the air-sea disequilibrium,

$$F_{dif} = G[(\frac{p_{atm}}{p_0})O_{2,eq}(T,S) - O_2](1 - f_{ice}), \tag{2.1}$$

where G (m s^{-1}) is the gas transfer velocity, p_{atm} (Pa) is the surface pressure, f_{ice} (dimensionless) is the fractional sea ice coverage, p_0 (Pa) is the standard atmospheric pressure, and $O_{2,eq}(T,S)$ (mol m^{-3}) is the saturated concentration of oxygen at the standard atmospheric pressure, which is a function of the local temperature and salinity (*Garcia and Gordon*, 1992). Cooling of the surface water increases the O_2 solubility, $O_{2,eq}(T,S)$, and the diffusive gas flux, F_{dif}. Throughout this manuscript all oxygen fluxes are set to be positive when oxygen is transfered into the ocean. At the same time, convective mixing tends to decrease surface O_2 concentrations due to the entrainment of subsurface waters that are relatively depleted in O_2; this in turn further enhances the air-sea disequilibrium. Stronger atmospheric winds also increase the efficiency of the air-sea gas transfer, G, which is typically parameterized as a power function of the near-surface wind speed. Furthermore, strong winds induce surface wave breaking that further intensifies the air-sea gas flux through the formation of air bubbles (*Monahan and Torgersen*, 1990; *Asher and Wanninkhof*, 1998; *Hamme and Severinghaus*, 2007). Relatively small bubbles can fully collapse to inject the air into the surface water, while relatively large bubbles may enhance diffusive gas ex-

change under increased pressure (*Fuchs et al.*, 1987; *Merlivat and Memery*, 1983; *Keeling*, 1993; *Hamme and Emerson*, 2002). Taken together, the intense air-sea interaction over the convecting ocean is likely to enhance the air-sea transfer of gases including oxygen.

The factors controlling the saturation state of the newly formed dense water masses in general and of LSW in particular, have far-reaching impact due to its control on the preformed O_2 (*Ito et al.*, 2004). In this region, surface oxygen does not fully equilibrate with the overlying atmosphere due to the intense mixing, relatively short surface residence time and finite air-sea gas exchange timescale, thus the newly formed water masses are undersaturated. The earlier study by *Najjar and Keeling* (2000) predicted a linear relationship between the cooling rate and the diffusive gas flux, but this theory did not include the effect of bubble-mediated fluxes and the convective entrainment. Enhanced bubble-mediated fluxes reduce the level of undersaturation and thus reduce the air-sea gradient that drives diffusive gas exchange. The response of the diffusive gas exchange weakens the O_2 uptake due to the reduced air-sea concentration gradient. It is not yet clear to what extent the effect of bubble-mediated flux is compensated by the reduction in the diffusive gas exchange under the influence of strong cooling and convective mixing. Thus it is crucial to determine the interactions between different components of the surface air-sea gas fluxes as well as the physical transport processes.

The objective of this study is to better quantify the relationship between the processes that control ocean oxygen uptake in convective areas. We do so through a theoretical analysis and a numerical investigation with a focus on the Labrador Sea. We present a new theory of air-sea oxygen fluxes and test it against a suite of numerical simulations with the goal of capturing the sensitivity of oxygen fluxes to the surface wind and buoyancy forcing. In section 2 we outline a theory of air-sea oxygen transfer that includes the effects of surface cooling, diffusive and bubble-mediated gas transfer, and entrainment of subsurface waters through convective mixing. In section 3 we introduce the model set-up and the numerical experiments performed to test our theory. We analyze the results of our simulations

and compare them with the theory in Section 4. Section 5 highlights main conclusions and presents further discussion points.

2.2 Theory

To illustrate the controls on the air-sea disequilibrium and the gas transfer, we examine the governing equation for abiotic oxygen omitting the biological sources/sinks,

$$\int_{-h_1}^{-h_2} (\frac{\partial O_2}{\partial t} + \mathbf{v} \cdot \nabla O_2 - \nabla \cdot \mathbf{K} \nabla O_2) dz = (F_{dif} + F_{inj})|_{z=-h_1}^{z=-h_2}, \tag{2.2}$$

where $\mathbf{v}$ (m s^{-1}) is the velocity field, and K (m^2 s^{-1}) is the tracer diffusion tensor parameterizing the effects of unresolved turbulent motions. F_{dif} and F_{inj} are the diffusive and bubble injection oxygen flux respectively. $F_{dif} = F_{inj} = 0$ when $z < 0$. For this theoretical calculation, we approximate the oxygen saturation to be a linear function of temperature over the small temperature ranges present at high latitude convection sites, $O'_{2,eq} = -A_1 T', (A_1 > 0)$, where A_1 (mol m^{-3} K^{-1}) is the linear coefficient. Combining equation (2.2) and the thermodynamic equation, we can write the equation for the saturation state, $\delta O_2 = O_2 - O_{2,eq}$, as follows.

$$\int_{-h_1}^{-h_2} (\frac{\partial \delta O_2}{\partial t} + \mathbf{v} \cdot \nabla \delta O_2 - \nabla \cdot \mathbf{K} \nabla \delta O_2) dz = (F_{dif} + F_{inj} + \frac{A_1 \mathcal{H}}{\rho c_p}) \Big|_{z=-h_1}^{z=-h_2}, \tag{2.3}$$

where $\mathcal{H}$ (W m^{-2}) is the surface heat flux (positive downward, $\mathcal{H} = 0$ when $z < 0$), and ρ and C_p are the density (kg m^{-3}) and the isobaric specific heat capacity (J kg^{-1} K^{-1}) of seawater.

2.2.1 Simplest case: diffusive gas exchange only

First, we consider an illustrative example where the air-sea gas and heat exchanges are restrained in a surface layer with a fixed depth h. We neglect the effects of horizontal advection and turbulent mixing, and assume that there is no ice and $p_{atm} = p_0$. Without the

entrainment and the bubble injection flux term, the equation for δO_2 equation becomes

$$h\frac{d\delta O_2}{dt} = -G\delta O_2 + F_T, \tag{2.4}$$

where $F_T = \frac{A_1 \mathcal{H}}{\rho c_P}$ represents the thermally driven capacity for O_2 uptake driven by a change in gas solubility following *Keeling et al.* (1993). F_T measures the change of oxygen saturation state induced by the solubility change due to heating $(F_T > 0)$ or cooling $(F_T < 0)$. This is a rough approximation, but it is sufficient to describe that there is stronger oxygen uptake under stronger and longer cooling. The analytic solution to equation (2.4) is

$$\delta O_2 = \frac{F_T}{G} - \left(\frac{F_T}{G} - \delta O_{2,0}\right) \exp\left(-\frac{G}{h}t\right), \tag{2.5}$$

where $\delta O_{2,0}$ is the initial oxygen concentration. This equation shows that δO_2 is relaxing towards the equilibrium. On a longer timescale relative to the diffusive gas exchange timescale of $\frac{h}{G}$, the initial condition is forgotten and the second term in equation (2.5) vanishes. The resultant, quasi-steady state flux is equivalent to the model of *Schudlich and Emerson* (1996) and *Hamme and Emerson* (2002). For wintertime deep mixing of O(1,000m), the magnitude of $\frac{h}{G}$ is O(100days) and the assumption of quasi-steady steady is unlikely to hold during convective seasons. Then, the cooling-induced surface undersaturation is facilitated by the lagged response of surface oxygen under the finite gas exchange rate (G) and the associated oxygen uptake is set to the rate of saturation increase via the temperature-solubility relationship (F_T) as described in Eq. 2.5.

2.2.2 The effect of convective vertical transport

Next we consider the the role of enhanced vertical mixing during convection (still in the absence of bubbles). This process plays a crucial role in setting the air-sea disequilibrium at the surface. Representing the vertical transport using a diffusive closure with a diffusive

coefficient (K), the equation for surface δO_2 becomes

$$h\frac{d\delta O_2}{dt} = -G\delta O_2 + \frac{K}{\Delta H}(\delta O_{2,deep} - \delta O_2) + F_T, \tag{2.6}$$

with $\delta O_{2,deep}$ being the background mean δO_2 in the deep layer (water below the surface layer) and ΔH being the distance between the middle point of the surface layer and the middle point of the deep layer. This is equivalent to a two-box model with a surface and deep box. Wintertime convection can be represented as an increased value of K. Because the water volume in the deep box is much larger than in the surface one, the change of $\delta O_{2,deep}$ is assumed to be much smaller and is effectively treated as a constant. Based on numerical model output, it is possible to estimate $\frac{K}{\Delta H}$ using the vertical transport and the mean δO_2 in the surface and the deep ocean. Assuming the quasi-equilibrium state, the left side of equation (2.6) vanishes:

$$\delta O_2(G + \frac{K}{\Delta H}) = F_T + \frac{K}{\Delta H}\delta O_{2,deep}. \tag{2.7}$$

The diffusive flux can be derived by multiplying both sides by $-G/(G + K/DeltaH)$:

$$F_{dif} = \frac{G}{G + \frac{K}{\delta H}}(-F_T - \frac{K}{\Delta H}\delta O_{2,deep}) = -\frac{1}{1+\eta}(F_T + \eta G\delta O_{2,deep}). \tag{2.8}$$

In this case the diffusive gas flux is determined by the rate of cooling and entrainment of subsurface waters. The relative importance of cooling-induced diffusive gas flux (F_T) and the entrainment-induced flux ($G\delta O_{2,deep}$) is measured by a dimensionless parameter, $\eta = \frac{K}{G\Delta H}$. When the convective mixing is stronger relative to the diffusive gas exchange ($\eta \gg 1$) the quasi-steady diffusive gas flux primarily depends on the air-sea disequilibrium supported by the entrainment of deep water, $F_{dif} \sim -G\delta O_{2,deep}$. In contrast, when the diffusive gas exchange is stronger relative to the convective mixing ($\eta \ll 1$) the quasi-steady diffusive gas flux primarily depends on the cooling-induced diffusive gas flux ($F_{dif} \sim -F_T$). Considering the integrated uptake for a cooling period (τ), the net O_2

uptake becomes

$$\Delta I = \int_0^\tau F_{dif} dt \simeq -\frac{1}{1+\eta}(F_T \tau + \eta G \delta O_{2,deep} \tau). \tag{2.9}$$

It implies that even when the total heat loss and the integrated thermal flux are held constant ($F_T \tau \sim constant$), the oxygen uptake increases with a longer period of cooling due to the cumulative effect of entrainment flux. This result remains valid even if the time dependence in δO_2 is included in the calculation. At the same time, the change of cooling strength will also affect η. This will also influence the O_2 uptake since it is scaled by $\frac{1}{1+\eta}$. However, it is not the dominant factor when compared to the effect of vertical transport.

2.2.3 The compensation between diffusive and bubble-mediated fluxes

When the representation of the bubble-mediated flux (F_{inj}) is included, the quasi-equilibrium solution for the diffusive flux becomes

$$F_{dif} = -G\delta O_2(t) \simeq -\frac{1}{1+\eta}(F_T + F_{inj} + \eta G \delta O_{2,deep}) = -\frac{1}{1+\eta}(F_T + F_{inj}) - \frac{\eta}{1+\eta} G \delta O_{2,deep}. \tag{2.10}$$

The first term is the response of the diffusive flux to the surface cooling and bubble-mediated flux, and the second term captures the influence of entrainment. This relationship indicates that the change in diffusive flux tends to compensate the effects of bubbles as explained below. We define the compensation rate (R) as

$$R = \frac{1}{1+\eta}, \tag{2.11}$$

which depends only on η. When the entrainment is strong relative to the diffusive gas exchange, the compensation ratio diminishes ($R \to 0$, no compensation) because the effect of strong entrainment maintains the surface oxygen concentration close to the subsurface

concentration, unaffected by the surface processes. On the other hand, if the entrainment is weak relative to the change in diffusive gas exchange, the perturbation will be fully compensated ($R \rightarrow 1$, full compensation) where the changes in the diffusive flux compensates the effect of bubble-mediated flux. The bubble-mediated flux can have direct impact on the total O_2 flux under the strong convective mixing ($\eta \gg 1$), but it would have a minimal impact on the total O_2 flux for weak convective mixing ($\eta \ll 1$). Figure 2.1 illustrates the mechanism. When the entrainment is relatively weak, the air-sea disequilibrium of O_2 is controlled by the three-way balance between bubble injection, diffusive gas exchange and thermally-induced solubility change. In this scenario, the addition of bubble injection raises the surface δO_2 such that the effect of the bubble-mediated flux is compensated by the weakening of the diffusive flux. In contrast, under a strong entrainment, the air-sea disequilibrium of O_2 is dominated by $\delta O_{2,deep}$. In this case, the additional O_2 influx from the bubble-mediated flux does not alter the diffusive flux, and it effectively increases the net O_2 uptake. While this situation is relatively rare for the stratified open ocean, it is essential for the oxygenation of deep waters during winter-time convection events in the polar oceans.

2.3 Model description and experimental design

To test our theoretical predictions we perform a suite of sensitivity experiments using the MIT General Circulation Model (MITgcm) (*Marshall et al.*, 1997a,b). The model is configured to allow non-hydrostatic dynamics to explicitly resolve deep convection, and the set-up is modified from *Jones and Marshall* (1993). In particular the model domain is a box with periodic boundary conditions in the x and y directions of 32 x 32 km with horizontal resolution of 250 m. The box has a uniform depth of 2 km with 41 z-levels whose thicknesses increases from 10 m at surface to 100 m near the bottom. The linear equation of state is used throughout this study. Both the viscosity and the tracer diffusivity are set to $2 \times 10^{-4}\ m^2\ s^{-2}$ with the time step of 10 s. The model is ice-free, and no background current is included. Convection is induced by applying a cooling patch at the sea surface

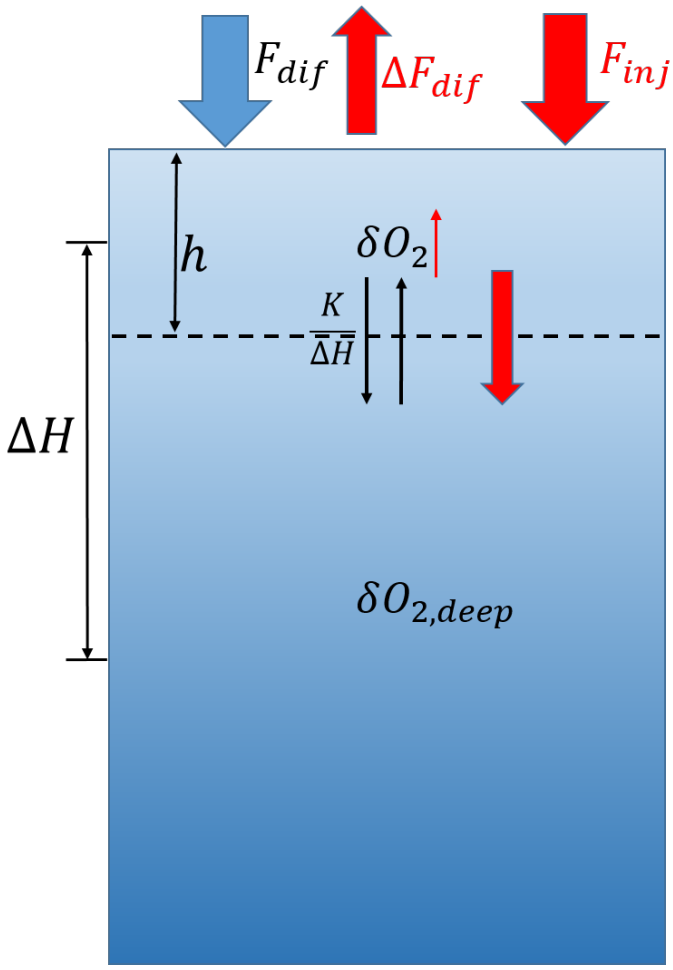

Figure 2.1: Schematic diagram of the compensation between the bubble-mediated flux and the diffusive flux.The red arrows indicate the change induced by the additional bubble-mediated flux. Part of the additional oxygen brought by the bubble flux is transported into deep ocean, and the rest will elevate the surface δO_2 level and further decrease the diffusive flux. The efficiency of the vertical transport is essential for the compensation rate.

within a disk of 8 km radius. To simulate the air-sea transfer of oxygen, a diffusive oxygen flux F_{dif} and a bubble injection flux F_{inj} are applied at the ocean surface (positive downward). The gas transfer velocity G is parameterized as $G = \alpha(\frac{u_{10}}{U_0})^2(\frac{S_c}{660})^{-0.5}$, where α is the closure coefficient, u_{10} is the 10 m wind speed, U_0 is the reference wind speed, and Sc is the Schmidt number (*Wanninkhof*, 1992; *Nightingale et al.*, 2000; *Ho et al.*, 2006). The curvature solubility of oxygen is applied through the water column following *Garcia and Gordon* (1992). The bubble-mediated gas exchange is parameterized assuming the injection of relatively small bubbles following *Monahan and Torgersen* (1990); *Asher and Wanninkhof* (1998); *Hamme and Severinghaus* (2007). The bubble injection flux is given by the equation

$$F_{inj} = \begin{cases} V_{inj}(1 - f_{ice})\frac{P_{atm}\chi_{O2}}{RT}(\frac{U_{10}-2.27}{U_0-2.27})^3 & U_{10} \geq 2.27ms^{-1} \\ 0 & U_{10} < 2.27ms^{-1} \end{cases}, \tag{2.12}$$

where V_{inj} = 9.1 $\times 10^{-9}$ m s^{-1} is a closure coefficient, χ_{O2} is the mixing ratio (0.21 for oxygen), R is the universal gas constant, $8.31 Jmol^{-1}K^{-1}$, T (K) is the absolute sea surface temperature, U_{10} (m s^{-1}) is the wind speed at 10 m above the sea surface and U_0 = 10.0 m s^{-1} is the reference wind speed. The closure coefficients used for the gas fluxes are identical to those of *Ito et al.* (2011). The modeled convection primarily depends on the extraction of buoyancy by the surface boundary condition. The amount of total buoyancy loss is set by the the intensity and the duration of the surface cooling.

Before performing the sensitivity experiments, we assess the ability of the model to reproduce the O_2 variability observed over the convecting region of the Labrador Sea. We use the observations taken by an autonomous float equipped with an oxygen sensor (WMO ID#4900611) as a validation dataset, and we evaluate how well our model reproduces observed profiles of temperature, salinity and oxygen during the 2005-2006 convective season. The CTD and oxygen measurements are obtained from the US-GODAE Argo data archive (http://www.usgodae.org/ftp/outgoing/argo/). Oxygen profiles from this particular

float are examined by *Kihm and Körtzinger* (2010) and we adopt their O_2 sensor calibration. Our simulation covers the convective season from the beginning of October 2005 to the end of April 2006, and observed surface momentum and heat fluxes for this period are used to force the model. The integration begins in the fall and ends in spring so that biological oxygen production is minimal, and the biological processes can be neglected. Both salinity and temperature distributions are used to reconstruct the stratification of the water column. The model is initialized with a horizontally uniform profile of temperature, salinity and oxygen taken from the float observation in October, 2005. Surface wind and buoyancy fluxes at the location of the float are interpolated from the NCEP-1 reanalysis (*Kalnay et al.*, 1996). Surface cooling and freshwater fluxes are applied over a circular region with radius of 8 km in the center of the model domain following *Jones and Marshall* (1993). Additional buoyancy forcing is applied as a restoring to the sea surface temperature and salinity from the Argo data. It is important to note that no restoring term is applied to the oxygen, so O_2 is allowed to evolve freely with the air-sea exchanges, circulation and mixing.

After the validation (Annalisa suggested to use control, I think she misunderstood this one?) simulation, further experiments are designed to test our theoretical framework. In all the sensitivity experiments, the salinity is set to be constant so that the stratification of the water column is only controlled by the temperature difference. For a given buoyancy loss over the winter season, there can be a compensation between the intensity and duration of the cooling. An intense cooling during a short period and a moderate cooling over a long period can both extract the same amount of buoyancy in the time integral sense, but their impact on the oxygen fluxes may differ. The theoretical prediction of our equation (2.9) is that a longer period of moderate cooling can be more effective in driving total O_2 uptake due to the cumulative effect of the entrainment of subsurface waters. At the same time equation (2.11) predicts that the bubble-mediated O_2 flux can effectively increase the net O_2 flux only in conjunction with the convective entrainment. In order to test these

Table 2.1: Parameters used for the sensitivity experiments. The heat flux is applied over the circular cooling patch. The choice of the cooling time and the heat flux ensures that the total heat loss over the cooling time is set to a constant across all the experiments. The 10 m wind speed is used only for the purpose of calculating the gas transfer coefficient (G) and the bubble-mediated gas flux (F_{inj}).

Run	period ($days$)	-Q ($W\ m^{-2}$)	$\lvert u_{10}\rvert$ ($m\ s^{-1}$)	Bubble
$c06w15$	6	4000	15	No
$c06w15B$	6	4000	15	Yes
$c06w05$	6	4000	5	No
$c06w05B$	6	4000	5	Yes
$c15w15$	15	1600	15	No
$c15w15B$	15	1600	15	Yes
$c15w05$	15	1600	5	No
$c15w05B$	15	1600	5	Yes
$c30w15$	30	800	15	No
$c30w15B$	30	800	15	Yes
$c30w05$	30	800	5	No
$c30w05B$	30	800	5	Yes
$c60w15$	60	400	15	No
$c60w15B$	60	400	15	Yes
$c60w05$	60	400	5	No
$c60w05B$	60	400	5	Yes

theoretical predictions, we design a suite of sensitivity experiments (Table 2.1) and examine the oxygen uptake and transport under different cooling conditions.

For all runs the simulation period is set to 90 days. The initial stratification in our model is maintained by the temperature gradient only. We use the annual mean climatological temperature profile of the central Labrador Sea as initial condition. Since the haline stratification is not included, the initial stratification in our experiments is weaker than observed, but the linkage between oxygen uptake and convection is not affected by this choice. The initial oxygen concentration is set to be saturated at the surface and linearly decreases towards the deep ocean. This implies that δO_2 is zero at the surface and decreases through the water column. We keep the total heat loss unchanged across all sensitivity runs, and examine the response of the net oxygen uptake to the magnitude of G, η and $\delta O_{2,deep}$. There are 4 sets of experiments evaluating the impact of varying the intensity and the duration of the cooling events (6, 15, 30 or 60 days) to achieve the same seasonally averaged heat loss.

The total heat loss is of comparable magnitude of the observational counterpart considering the mean net heat flux is about 400 W m^{-2} (upward) during the winter (DJF) in the central Labrador Sea. We also perform experiments using relatively strong and weak magnitudes of G and F_{inj} by using different 10 m wind speeds of 5 and 15 m s^{-1}. In our experiments, the 10 m wind speed only affects the gas exchange coefficients and and does not alter the circulation or the air-sea buoyancy fluxes.

2.4 Results and discussion

2.4.1 Model evaluation

Figure 2.2 shows the simulated and observed profiles of temperature, salinity , oxygen and δO_2. The vertical profiles evolve significantly over the simulation period primarily reflecting the deep convection event. The upper ocean thermocline rapidly cools and deepens from December to February, and the corresponding increase in oxygen concentration is captured reasonably well. δO_2 is always negative since the oxygen is under-saturated during the whole convection event. Changes of $O_{2,eq}(T, S)$ and O_2 both affect the evolution of δO_2, but the contribution of O_2 is dominant here. Ventilation brings oxygen into the deep ocean and increases δO_2. The model tends to overestimate mid-depth oxygen concentration by about 3% at $\sim$1000 m, which may indicate that the simulated convective mixing might be supplying oxygen at a slightly higher rate than observed.

Figure 2.3 shows a more critical validation of the temporal evolution of the δO_2 at various depths (195 m, 495 m and 950 m). In the near-surface waters (195 m) the sudden increase in δO_2 indicates the erosion of the upper thermocline and the onset of convective mixing from December to January. The onset of convection occurs about 2-3 weeks earlier in the model than in the observations. Convective mixing reaches 495 m in late January and 950 m in late March. Despite the earlier onset of convection, the model reproduces δO_2 before and after the convective event reasonably well. Considering that we neglected lateral advection in our model, and that the Argo float is moving, we can conclude that our

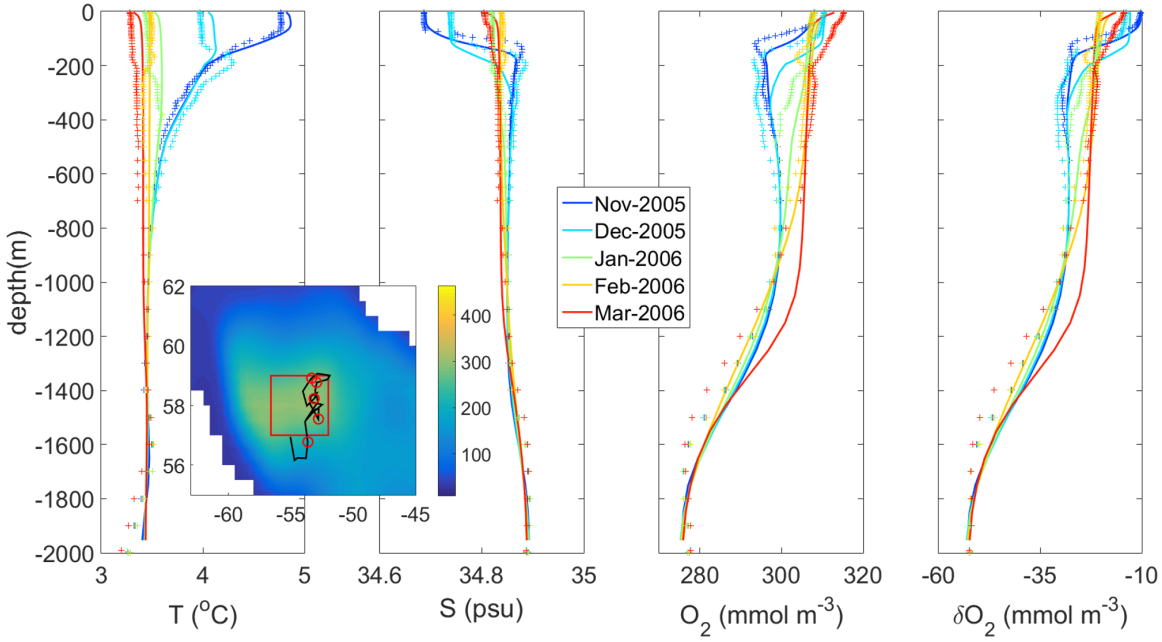

Figure 2.2: Mean vertical profiles between Nov., 2005 and Mar., 2006 from the model validation run (solid lines) and Argo observations (plus).The black line in the small map indicates the float track between Oct., 2005 and Apr., 2006. The red circles are the positions where the the profiles showed in the figures are measured. The background contour is the climatological mixed layer depth in March (*Johnson et al.*, 2012).The red box indicates the central Labrador Sea region where the deep convection events usually take place (*Yashayaev*, 2007).

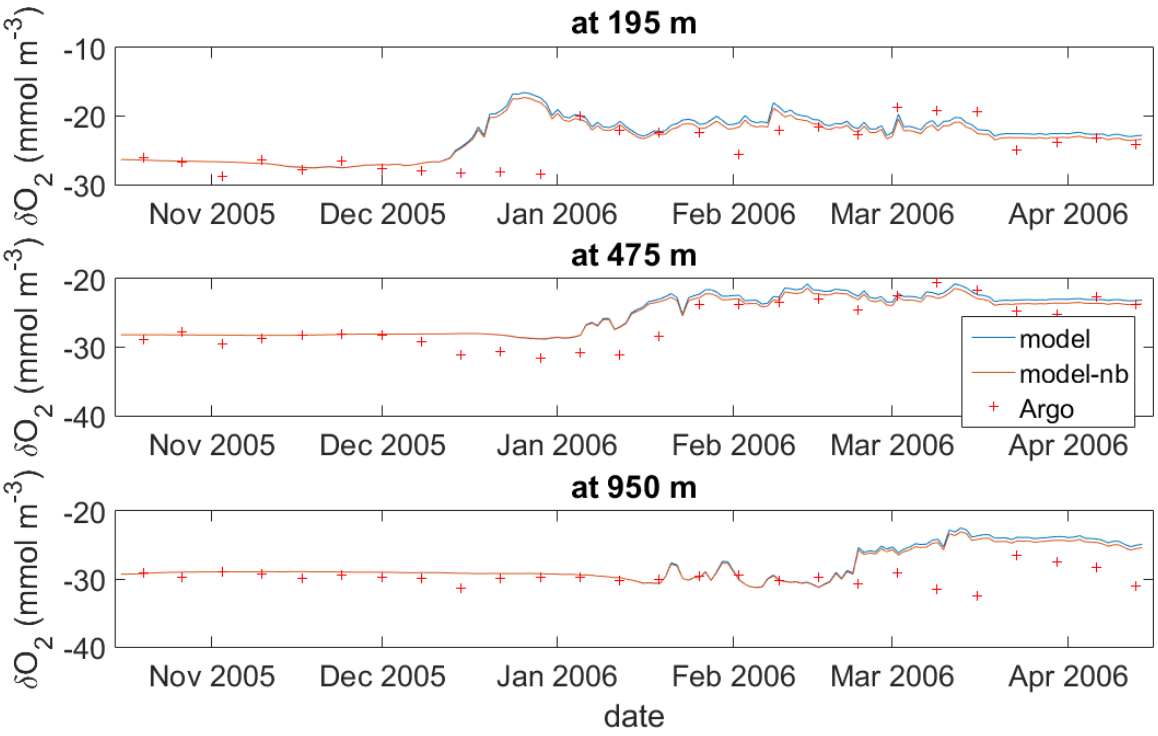

Figure 2.3: Time series of $\delta O2$ at different depths in the model (with or without bubble injection flux) and Argo observations. Note that the y-axises show different range in each panel.

model is skillful in simulating the vertical oxygen transport during deep convection events.

Encouraged by the model validation, we then perform the suite of sensitivity runs described previously to study what controls the vertical transport of oxygen during deep convection events. In particular, we test the two hypotheses put forward in our theory: the total oxygen uptake increases with a longer period of cooling even when the total heat loss is held constant, and the diffusive flux can partially compensate the bubble injection.

2.4.2 Standard run: deep convection and O_2 transport

Here we closely describe the time evolution of the standard run ($c30w15B$ in Table 1). Briefly, this integration uses a 30-day cooling period with 800 W m^{-2} heat flux, a strong gas exchange coefficient (equivalent of 15 m s^{-1} wind) and includes the bubble injection flux. This parameter set is analogous to the climatological surface forcing of the central Labrador Sea, and this run exemplifies the evolution of a deep convection event in agree-

ment with previous results by *Jones and Marshall* (1993). The surface cooling weakens the upper ocean stratification rapidly, and violent mixing takes place when it becomes statically unstable (Figure 2.4). Strong ascending and descending currents penetrate to more than 1500 m (for the simulation with strongest cooling, the convection can reach the bottom) and form narrow plumes within the cooling patch. This mixing process drives the heat and oxygen transport between the surface and the deep ocean and builds a "chimney" of homogeneous fluid (Figure 2.5 and 2.6). As convection continues, a horizontal geostrophic current develops because of the rotation effect, and eddies begin to develop horizontal meanders at the density front. With the cessation of surface cooling, the vertical motion halts immediately. The remaining horizontal advection and the geostrophic eddies tend to homogenize the water laterally and eventually lead to the disintegration of the chimney-like structure. The restratification of the water column shuts down the communication between the undersaturated deep waters and the atmosphere. The change in oxygen concentration is therefore confined within the surface 100 m due to the reduced size of the reservoir in contact with the atmosphere; the end result is that the surface water reaches saturation quickly ($\sim$5 days), and the oxygen update stops.

The time-depth diagram of Figure 2.7 visualizes the progression of the vertical mixing and the tracer tendencies as the surface water is cooled. The extent of the cooling tendency deepens as the cooling continues. The mass exchange between upper and deeper layers decreases the oxygen in the upper layers and increases it in the deeper layers as shown by the vertical structure of the O_2 tendency. The evolution of upper ocean O_2 is determined by the net effect of the vertical mixing and the incoming surface flux. Immediately after the cooling and buoyancy loss stop, surface oxygen increases towards saturation and eventually reaches super-saturation when there is a strong bubble injection. The evolution of the air-sea disequilibrium of oxygen δO_2 is controlled by the combination of temperature-induced saturation change, air-sea exchange and transport processes. For most of our experiments, intense cooling forces the δO_2 to decrease, maintaining the increasing downward diffusive

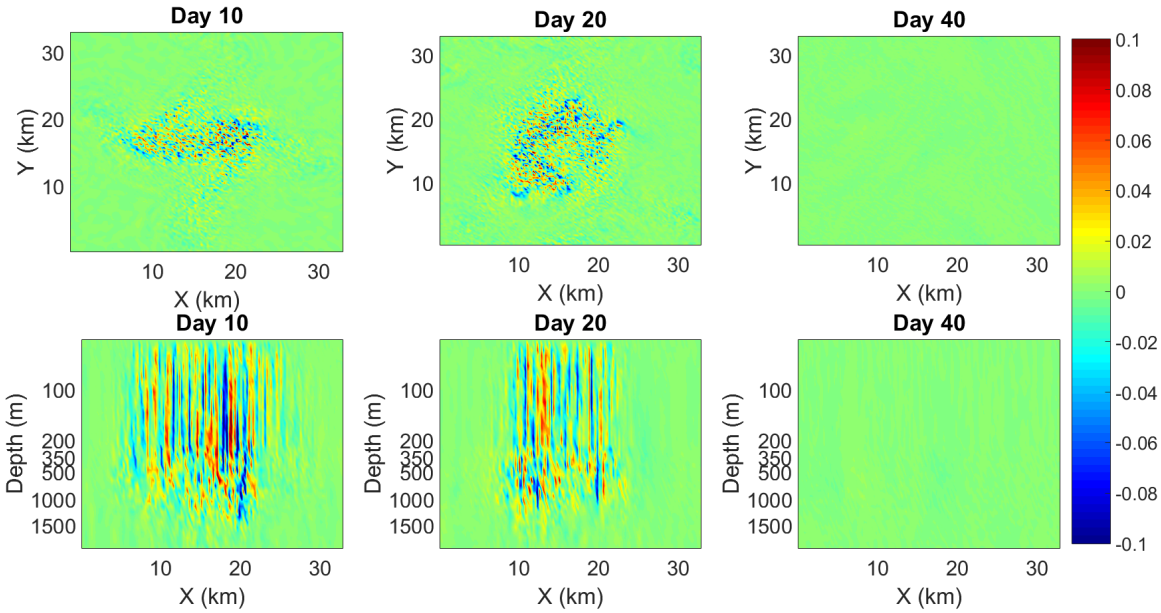

Figure 2.4: Vertical velocity (unit: m s^{-1}) in experiment $c30w15B$ at 10 days (left 2 panels), 20 days (middle 2 panels) and 40 days (right 2 panels). Note that the vertical axis is stretched to visualize the detailed structure of the upper 200m of the water column. The upper panels show horizontal sections at 100 m and the bottom panels show vertical sections along Y = 16.375 km.

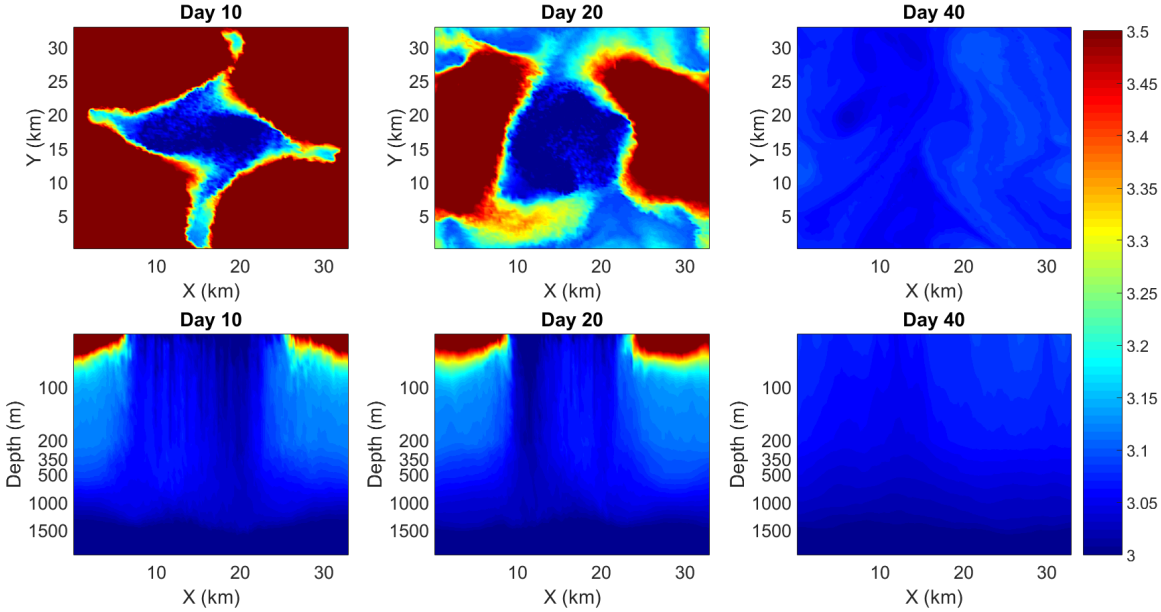

Figure 2.5: Temperature (unit: ^{o}C) sections in experiment $c30w15B$ at 10 days (left 2 panels), 20 days (middle 2 panels) and 40 days (right 2 panels). Note that the vertical axis is stretched to visualize the detailed structure of the upper 200m of the water column. The upper panels show horizontal sections at surface and the bottom panels show vertical sections along Y = 16.375 km.

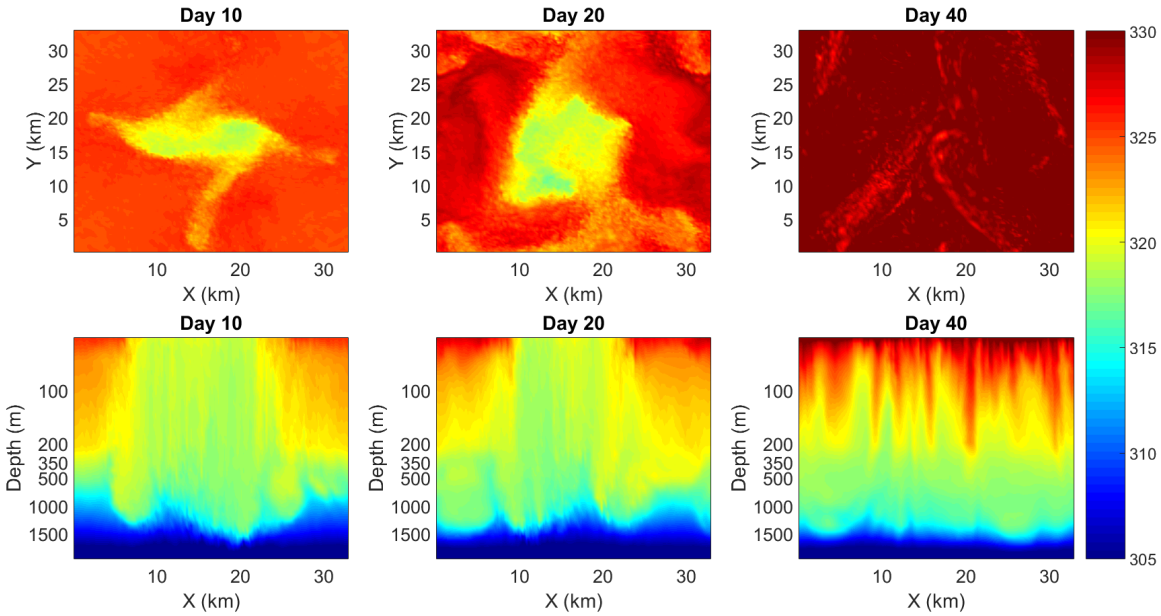

Figure 2.6: Oxygen concentration (unit: mmol m^{-3}) in experiment $c30w15B$ at 10 days (left), 20 days (middle) and 40 days (right). Note that the vertical axis is stretched to visualize the detailed structure of the upper 200m of the water column. The upper panels show horizontal sections at surface and the bottom panels show vertical sections along Y = 16.375 km.

oxygen flux. The evolution of δO_2 in the interior ocean is eventually controlled by the oxygen lateral transport.

2.4.3 Testing the theoretical prediction: controls on the net O_2 uptake

Here we examine the theoretical prediction that the net O_2 uptake increases with the duration of the cooling period for a given total heat (buoyancy) loss. To evaluate the overall differences among the sensitivity runs performed, we compare the final states of each experiment (Figure 2.8). The simulations cover varying cooling rates, gas exchange coefficients and bubble fluxes to examine the factors determining the net O_2 uptake. Net O_2 uptake increases with the magnitude of the gas exchange coefficient (G) as expected. A greater G increases the diffusive fluxes and therefore it increases the oxygen concentration in the upper layers. The impact of a longer cooling period is visible in Figure 2.8 where the profiles of O_2 and δO_2 with longer duration (red and magenta lines) are elevated above the depths

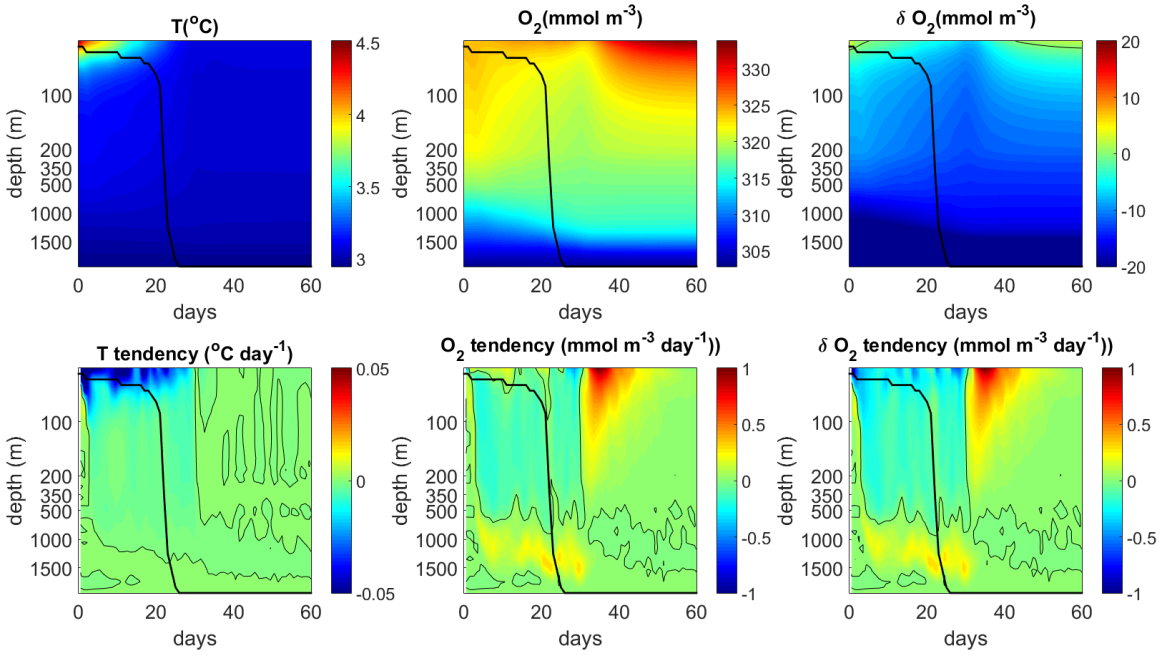

Figure 2.7: Horizontally averaged profiles and their tendency evolution for experiment $c30w15B$. The right most 2 panels show temperature and its tendency. The middle 2 panels show the oxygen concentration and the left most 2 panels are the δO_2. In all panels time in days from the beginning of the simulation is on the x-axis (only day 0-60 was showed here) and depth is on the y-axis. Thin Black contour lines indicate the value of 0, and the thick black line is depth of mixed layer based on the temperature difference ($\Delta\theta < 0.2^oC$). Note that the vertical axis is stretched to visualize the detailed structure of the upper 200m of the water column.

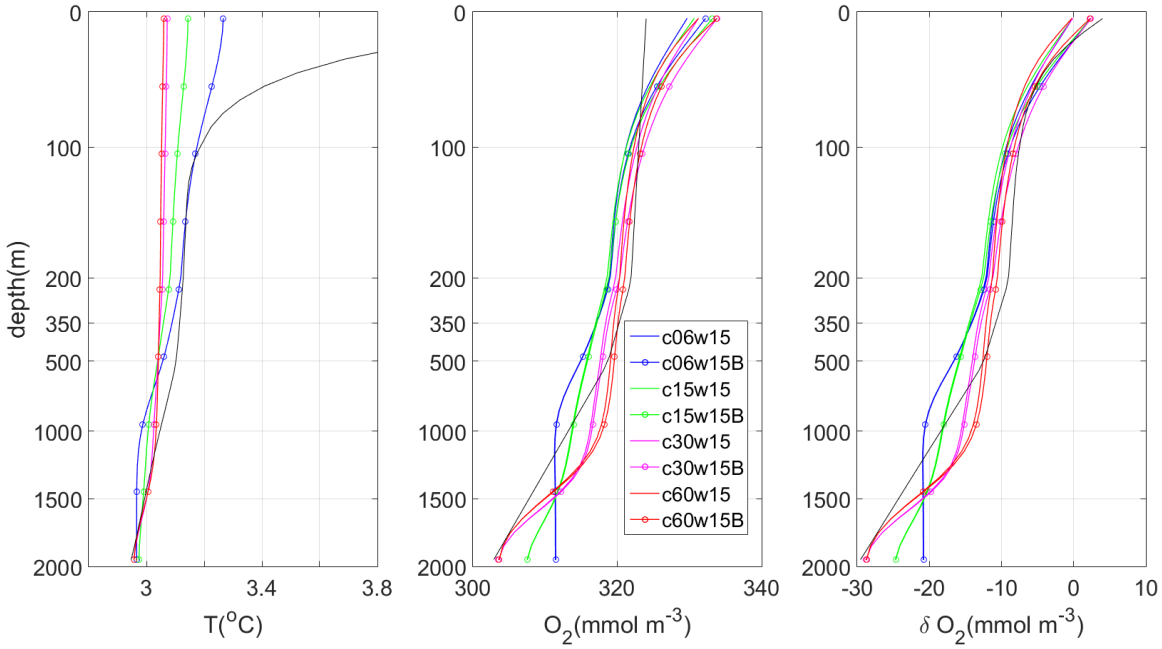

Figure 2.8: Horizontally averaged profiles for different experiments at the end of each simulation. The left panel is temperature, the middle one is oxygen and the right one is δO_2. The black line in each panel represents the initial condition. Only the experiments with 15 m s^{-1} wind speed are shown here, the structure of the profiles in the 5 m $s-1$ experiments are similar.

shallower than 1,500m relative to the runs with shorter duration (blue and green lines). Intense cooling over a shorter period causes the convection to reach deeper waters (blue line) showing higher concentrations below 1,500m. The extended cooling period - despite the weaker intensity of the surface heat fluxes - maintains convection and vertical mixing for longer, extending the exposure of the deep water to the air-sea interface, and transporting surface, O_2-rich waters to the deep ocean.

Our sensitivity experiments are consistent with the theoretical prediction that, for a given constant total heat loss ($F_T\tau = const$), the amount of oxygen absorbed increases with the duration of the convective season. The positive impact of the cooling period on the net O_2 uptake is evident in Figure 2.9, where the time-integrated O_2 uptake for all sensitivity runs is plotted and compared. For the same value of G, the temporally integrated O_2 uptake increases with the cooling period, generally supporting the theoretical prediction. Quantitatively the theoretical estimate of O_2 uptake using equation (2.9) captures the

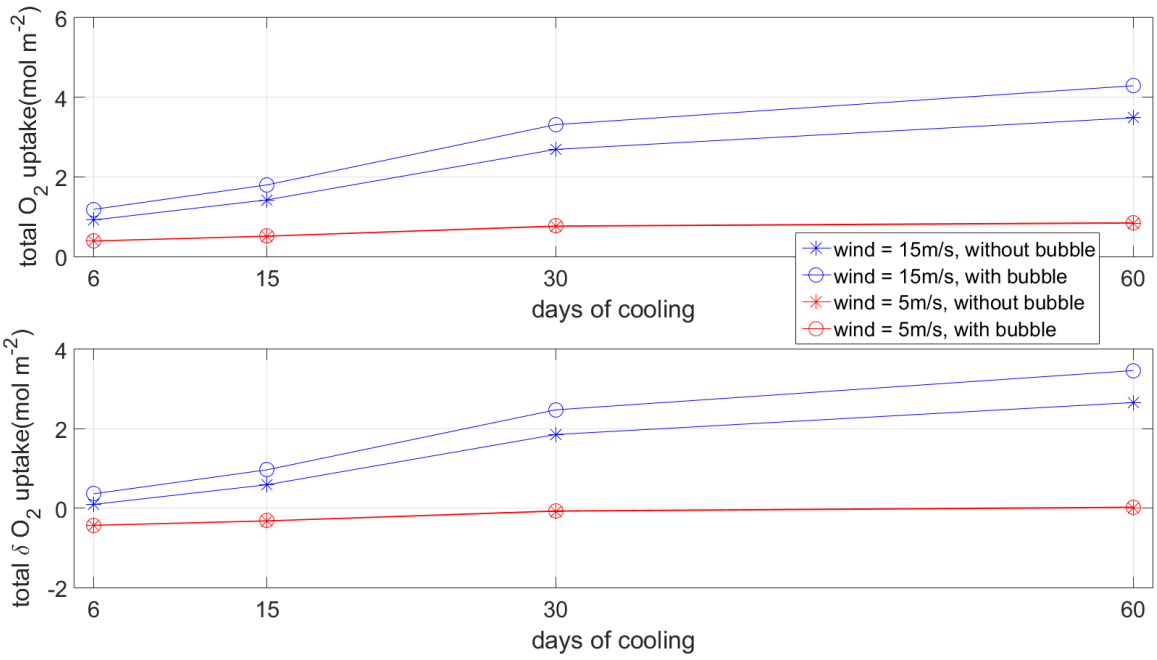

Figure 2.9: The total air-sea flux for O_2 (top) and δO_2 (bottom), which includes the change of solubility due to surface heat flux.The total flux is integrated through the whole 90-day simulation. The x-axis indicate the total cooling days applied to the experiments.The experiments without bubble-mediated fluxes are indicated by the star, and the ones with bubble fluxes are showed by the circle. The red lines indicate the experiments under weaker wind, and the blue lines are the experiments with stronger wind.

parameter sensitivity reasonably well but the calculated magnitude of fluxes and air-sea disequilibrium can vary significantly from the simulated values because of the several assumptions made. First of all, we assumed that the system is always at quasi-equilibrium and can be described by a linear theory, but this may not be the case for intense cooling scenarios. Second, the oxygen entrainment is assumed to be constant during the whole cooling period, but in the simulation or reality deep convective events have a more complicated evolution, and the exchange rate is likely to change during their lifespan.

2.4.4 Testing the theory: Bubble-diffusion compensation

We now examine the theoretical prediction that the effect of bubble-mediated flux can be compensated by a reduction in diffusive gas exchange depending on the strength of vertical mixing. The parameterization of the bubble injection flux in equation (2.12) is proportional

to the cubic power of the near-surface wind speed, thus the impact of the bubble flux can rapidly increase with high wind speeds. In our parameter choice, such effect can become comparable in magnitude to the diffusive flux under high wind conditions.

In our sensitivity experiments, the bubble mediated flux can significantly increase the net oxygen flux, but the bubble effect is partially compensated by the weakening of the diffusive flux (Figure 2.10). As predicted by the theory (equation (2.11)) the compensation is weaker when the cooling is more intense (shorter cooling period) because the entrainment of subsurface δO_2 prevents the increase of surface δO_2. In other words, the oxygen flux is close to the linear sum of the diffusive flux and the bubble injection. Overall, more than 50% (52%$\sim$65%) of the bubble injection flux is compensated by a reduction in diffusive flux, in good agreement with the estimate from our theory. Using our model setting, η is found to vary between 0.40 to 0.90 from the weakest to the strongest cooling cases, indicating compensation rates of 52-71%. Therefore more than half of the bubble effect is compensated by the weakened diffusive flux.

2.5 Conclusion

In the ocean the physical supply of oxygen to deep and intermediate waters occurs through deep convective activity at high latitudes. We have investigated the processes that control the oceanic uptake of oxygen during the convective season. Our results suggest that both the intensity and the duration of the buoyancy forcing contribute to the overall oxygen uptake. The intensity of the cooling controls how deep the O_2-rich surface waters can be mixed downward; the duration of convective mixing controls the cumulative O_2 uptake by sustaining the entrainment of subsurface, undersaturated waters. *Najjar and Keeling* (2000) suggested a linear relation between the rate of cooling and air-sea O_2 flux, but the strict application of this theory to the net O_2 uptake is problematic because it only accounts for the solubility change due to the air-sea heat flux without considering the entrainment of subsurface waters and the bubble-mediated fluxes. The bubble-mediated flux is not additive

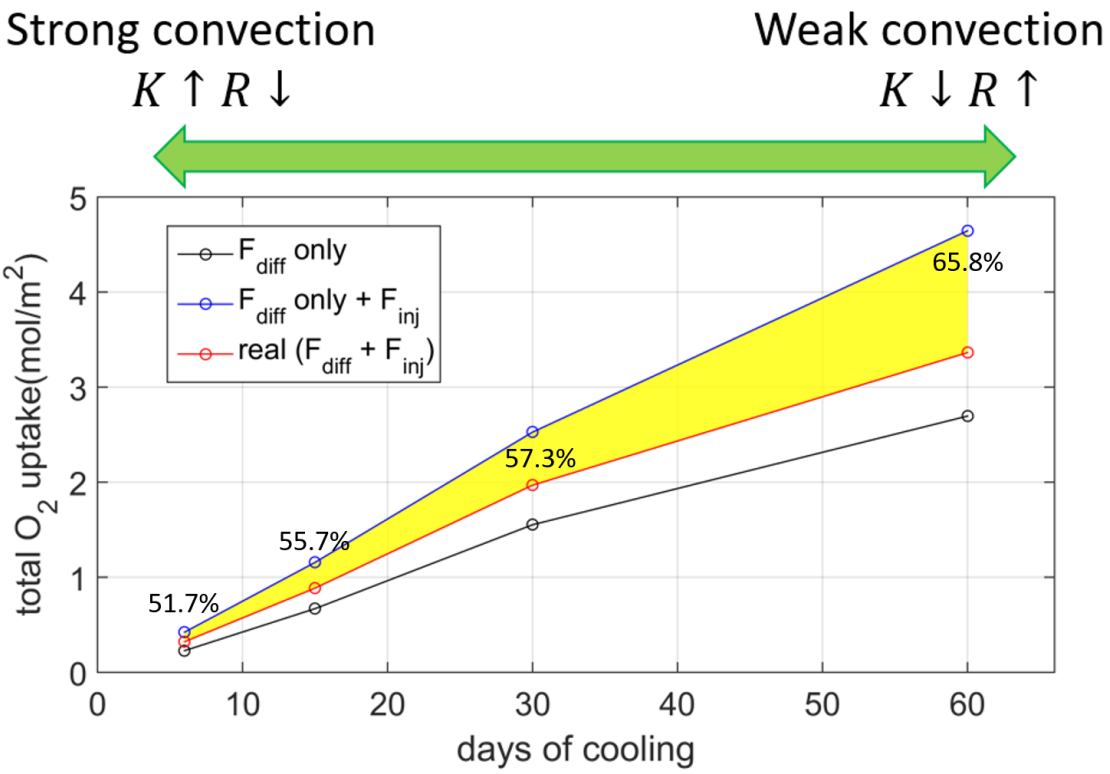

Figure 2.10: Compensation between the diffusive O_2 flux and the bubble injection (strong wind cases). The black line shows the total diffusive fluxes into the ocean for different cooling experiments when no bubble injection is included. The blue line shows the potential total fluxes when the bubble injection is included in the absence of any compensation. The red line shows the actual total fluxes (with compensation) and the yellow shading highlights the compensation.To be consistent with equation (2.11), only the fluxes during the convection period are included.The percentages around corresponding data points are the compensation rates.

to the total O_2 flux due to the compensation between the bubble and diffusive fluxes.

We examined numerous experiments where the total buoyancy (heat) loss is held constant, and found that the net O_2 uptake over the convective season can vary significantly. In fact, the longest cooling experiment (60 days) can bring about 3 times more oxygen into the ocean than the shortest cooling experiment (6 days) even if the total buoyancy (heat) loss is the same. The net O_2 uptake depends on both the magnitude of the total heat loss during the convective season and on the period over which the water that participates in convection is exposed to the air-sea interface. In reality, the rate of cooling is correlated with the surface wind speed, which increases the efficiency of air-sea gas exchange and further amplify the difference.

Additionally, the air-sea oxygen flux is significantly modulated by the interaction between the diffusive and bubble-mediated gas fluxes. In stratified condition, the bubble-mediated gas flux does not significantly contribute to the net O_2 uptake due to the compensation by the diffusive gas flux whenever the entrainment of subsurface water is weak. However, in the case of strong mixing the bubble-mediated flux can significantly increase the net oxygen uptake because the entrainment of subsurface waters maintains the undersaturation of the surface waters.

In our analysis we omitted several important processes such as biological O_2 production, respiration, the impacts of sea-ice on the circulation and gas exchange, and the role of large-scale horizontal transport. Further research is clearly needed to generalize our simple theory applicable to a more comprehensive model for better representation of realistic situations. Our numerical experiments only included a representation of the bubble injection flux relevant to relatively small bubbles that completely collapse in the water, and a different parameterization may be necessary to represent non-collapsing bubbles. However, the overarching conclusion that a compensation exists for the air-sea gas transfer between the diffusive and bubble-mediated fluxes is likely to hold as long as the bubble-mediated flux provides additional influx of O_2 to the surface water. Bubble formation is ubiquitous across

the global oceans, but it does not necessarily contribute to the net air-sea exchange. The polar oceans are exceptional that the bubble effect can increase the net air-sea O_2 flux, and the convective mixing transports it into the intermediate and deep waters.

In a warming climate, the physical transport of O_2 into the interior ocean is predicted to decline due to the thermally-induced reduction of gas solubility and the increasing ocean stratification that may inhibit convective mixing of O_2-rich surface waters. Our results point to additional factors that may regulate the O_2 uptake into the polar oceans. The O_2 uptake depends not only on the net heat flux during the convective season but also on the intensity and the length of the cooling period. The bubble-mediated gas flux can be particularly effective in the convecting ocean because the compensation from diffusive gas exchange is relatively weak such that the two components of the gas fluxes together drive the air-to-sea transfer of O_2. These results suggest the importance of continuing observations of gas tracers in regions of dense water formation to better understand the underlying processes and the linkages to climate trends and variability.

CHAPTER 3

CONTROL OF THE OXYGEN TO OCEAN HEAT CONTENT RATIO DURING DEEP CONVECTION EVENTS

Manuscript in preparation as

[1] Sun, D., T. Ito, A. Bracco (2020), Control of the oxygen to ocean heat content ratio during deep convection events. In preparation.

Abstract

Earth System Models predict a decline of dissolved oxygen in the ocean under a warming climate. The loss of oxygen per unit heat uptake is defined as the oxygen to ocean heat content (O_2-OHC) ratio. This quantity encapsulates the biogeochemical response to the climate warming. Observational studies of air-sea fluxes as well as ocean oxygen inventory suggest that the magnitude of O_2-OHC ratio is several fold larger than that calculated from the temperature-solubility relationship, however, it is not yet clear what controls the long-term, global-scale mean O_2-OHC ratio. This study focuses on the Labrador Sea, a major site of deep water formation in the North Atlantic Ocean, and aims at understanding the factors controlling the O_2-OHC ratio during deep convection using models of different complexity. Both theoretical predictions based on a one-dimensional convective adjustment model and results from a regional circulation and biogeochemistry model suggest that the total oxygen uptake increases with stronger cooling, and longer cooling periods allow more oxygen into the ocean for a given total heat loss. The numerical model captures the observed large-scale observation of O_2-OHC ratio, and agrees broadly with the prediction by the simpler model. Moreover, the effect of small, collapsing bubbles in the air-sea gas transfer significantly increases the O_2-OHC ratio, especially during intense convective events. The lateral transport and regional biological productivity can pre-condition the vertical gradients of oxygen and temperature, that are important for the O_2-OHC ratio under a

different climate.

3.1 Introduction

Dissolved oxygen (DO) is an ocean tracer essential to the well-being of the marine ecosystem. (e.g., *Codispoti*, 1995; *Morel and Price*, 2003; *Pörtner and Knust*, 2007). However, both projections by Earth System Models (ESMs) and observational evidences suggest that DO is declining in the global oceans (*Bopp et al.*, 2002; *Matear et al.*, 2000; *Plattner et al.*, 2002; *Keeling et al.*, 2010; *Schmidtko et al.*, 2017). Warming has two main effects on the oceanic oxygen inventory. Firstly, the increasing temperature directly reduces oxygen solubility. Secondly, warming of the upper ocean increases the stratification. This has two consequences: on one hand, it weakens the exchange between the well-oxygenated surface water and the ocean interior, on the other hand, it reduces the upwelling of nutrients from the deep ocean therefore increasing the subsurface DO by reducing the export production from surface. Overall, however, stronger stratification decreases the global oceanic DO (*Keeling and Garcia*, 2002). The net result is that warming and increasing stratification work together to deplete oxygen in the ocean (*Bopp et al.*, 2002; *Plattner et al.*, 2002), and this complicates the estimate of the oxygen to ocean heat content (O_2-OHC) ratio. *Keeling and Garcia* (2002) suggested that the natural O_2-OHC ratio occurs in a wide range from -2 to -10 $nmolO_2\,J^{-1}$ based on regional observations. Larger ratios are typically found at higher latitudes and when averaged over longer time scales. ESMs have predicted that the O_2-OHC ratio at the end of this century in global warming scenarios will be between -5.9 and -6.7 $nmolO_2\,J^{-1}$ (*Keeling et al.*, 2010). *Ito et al.* (2017) estimated the O_2-OHC ratio of the upper ocean (0-1000 m) as -8.2 $\pm$ 0.66 $nmolO_2\,J^{-1}$ based on reanalysis data from 1958 to 2015. For the surface layers, the O_2-OHC ratio follows the dependency of solubility on temperature change, but when deeper layers are included, the ratio is much larger than what can be explained by the solubility change, which can only explain 20% of the ratio (Figure 3.1) for the upper 1000 m of the global ocean. The remaining portion must

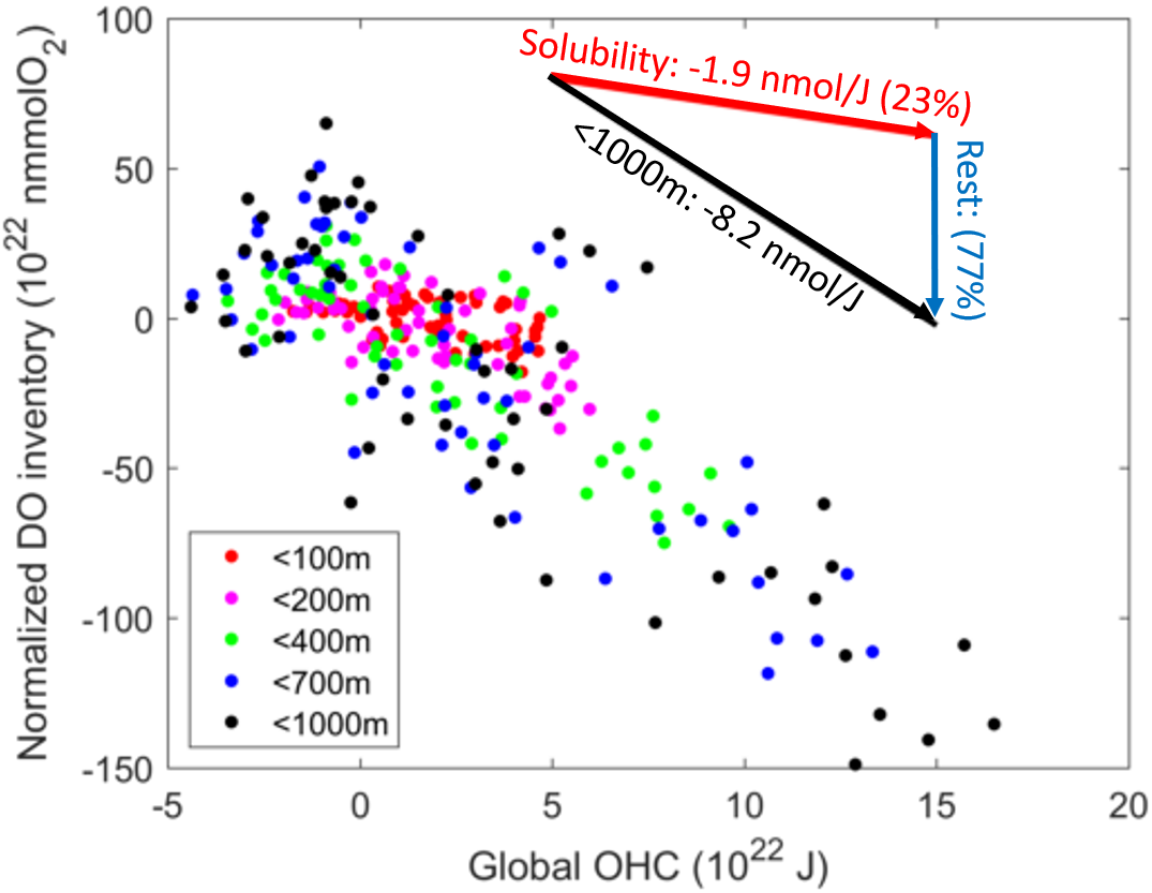

Figure 3.1: Normalized oxygen inventory as a function of global OHC inventory from 1858 to 2013 with the 1960-1970 decadal average removed from *Ito et al.* (2017). Scatters with different colors indicate the oxygen inventories and OHCs calculate above different depth. The black arrow shows the slope between oxygen inventory and OHC for the upper 1000 m in global ocean. The red arrow shows the slope can be explained by the change of solubility and the blue arrow shows the residual.

result from the ocean circulation and biology *Keeling and Garcia* (2002). In this work, we will further investigate the O_2-OHC ratio by directly examining the relation between heat loss and oxygen uptake at the time when water masses are formed, and by addressing what factors can constrain this ratio.

For the ocean interior, the oxygen is by large supplied by high latitude subduction and deep convection in the cold seasons. Large amount of oxygen are advected to the deep ocean at locations where deep mixing happens (*Körtzinger et al.*, 2004). Near-surface physical processes determine the DO content at the time of deep water mass formation,

termed as preformed oxygen (*Ito et al.*, 2004). While cooling raises oxygen solubility, convective mixing and entrainment lower the preformed oxygen, overall generating a strong oxygen flux into the ocean. The heat loss and oxygen uptake during this process can set the ratio between the preformed oxygen and OHC. In this study, the Labrador Sea, where strong convective mixing (*Marshall and Schott*, 1999; *Pickart et al.*, 2002) can happen from the surface to depths at times exceeding 2,000 m in winter (*Lazier*, 1980; *Clarke and Gascard*, 1983; *Gascard and Clarke*, 1983; *Lazier et al.*, 2002; *Yashayaev et al.*, 2007; *Yashayaev*, 2007), is chosen as representative location to understand the relation between oxygen flux and surface buoyancy forcing at water mass formation. After convection takes place in winter, the well oxygenated Labrador Sea Water (LSW) spreads across the northwest Atlantic between 1,000 and 2,200 m (*Talley and McCartney*, 1982; *Hall et al.*, 2007). Studying the O_2-OHC ratio of the newly formed LSW, thus, is important for understanding the O_2-OHC ratio in the entire North Atlantic, and the underlying mechanism is relevant to any other open ocean location where deep convection occurs.

In this work, we investigate the sensitivity of oxygen uptake to heat loss using a hierarchy of models. In section 2 we develop hypotheses using a one-dimensional (1-D) convective adjustment model with surface oxygen flux forced by surface cooling. Based on this idealized model, we further derive theoretical predictions for the O_2-OHC ratio. In section 3 we design a set of numerical simulations to test our theory. The results of the simulations is analyzed in Section 4. Section 5 summarizes the main findings.

3.2 Theory and hypotheses

The schematic diagram (Fig 3.2) illustrates the processes at play. Heat loss in the surface ocean (Q) is the principal driver of ocean oxygen uptake (*Sun et al.*, 2017).

First, atmospheric cooling causes the upper ocean temperature to decrease, and associated solubility to increase. This causes surface undersaturation, and diffusive gas transfer increases oxygen uptake.

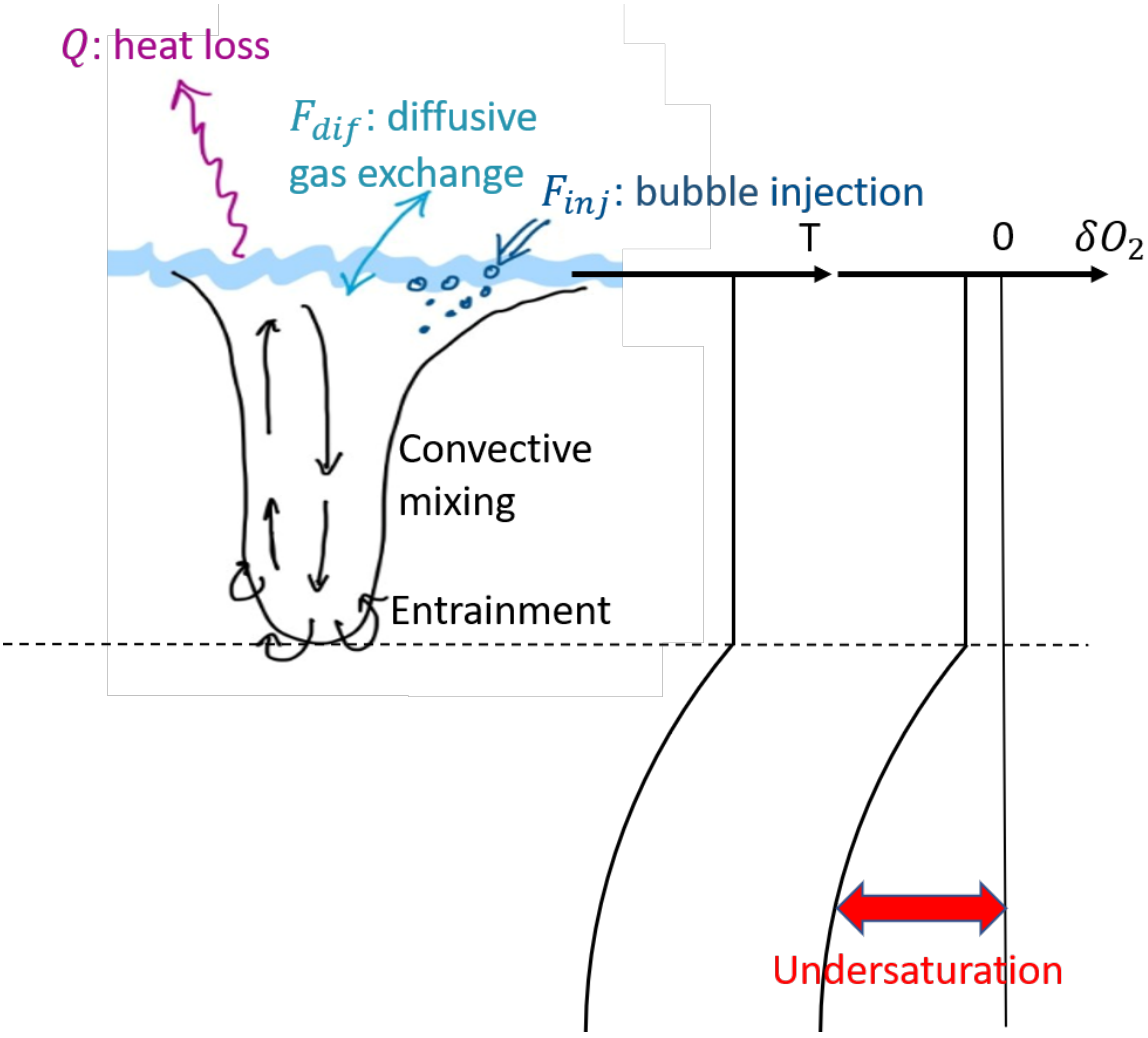

Figure 3.2: Schematic diagram of physical processes that control oxygen fluxes during winter time convection. δO_2 is a measure of saturation, and is generally negative in the interior ocean due to the cumulative effect of respiration.

Secondly, cooling causes convective instability. The intense vertical mixing brings up deep waters that are undersaturated in oxygen due to the cumulative effect of respiration. This further enhances the oxygen undersaturation and uptake.

Thirdly, the intense vertical mixing increases the effect of bubble-mediated oxygen uptake. *Sun et al.* (2017) demonstrated the convective enhancement of the bubble-mediated oxygen flux. When vertical mixing is weak, the bubble flux is largely compensated by the reduction of the diffusive gas exchange due to its tendency to cause surface supersaturation. Under strong vertical mixing, the saturation state of surface water is not influenced

by the bubble injection, rather it is dictated by the entrainment of the subsurface waters. Thus the diffusive and bubble gas flux together contribute to the oxygen uptake without compensation.

Sun et al. (2017) also demonstrated that, for a given amount of heat loss, the net oxygen uptake depends on the duration and intensity of the cooling event, and details of cooling conditions led to different O_2-OHC ratios. A weaker cooling spread over a long period can eventually bring more oxygen into the ocean because of higher level of air-sea equilibration. However, intense cooling over a short period can enhance the oxygen uptake through bubble injection without compensation with the diffusive flux. This implies that including the bubble injection allows for a higher level of the O_2-OHC ratio in the regions with strong cooling over relatively short periods.

We construct a simple vertical 1-D model to examine the factors that control O_2-OHC ratio during deep convection. In this idealized model, we neglect horizontal transport and assume that vertical mixing is induced by convection. All properties are assumed to be well mixed within the mixed layer, but all properties remain unchanged below the mixed layer. Mixed layer depth (MLD) only increases when the stratification is unstable at the bottom of the mixed layer (i.e., the water in the mixed layer is less buoyant than the water beneath).

3.2.1 Heat budget and mixed layer depth

First, for simplicity sake, we consider the heat budget and MLD of the water column where stratification is controlled entirely by the temperature gradient. The initial potential temperature profile is $T_0(z)$ ($z \leq 0$, $z = 0$ is the surface). $T_0(z)$ needs to be monotonically decreasing with depth to remain stably stratified. As the water in the mixed layer cools down, MLD, indicated as $H(t)$, will increase.

Potential temperature in the mixed layer is uniform and its value is set equal to the initial profile at the base of the mixed layer, $T(t) = T_0(-H)$. The heat loss at the surface

equals the time rate of change in the heat content so that:

$$\begin{aligned} Q(t) &= \rho_0 C_p \frac{d}{dt}\left\{ T(t)H(t) + \int_{-H_{max}}^{-H(t)} T_0(z)dz \right\} \\ &= \rho_0 C_p \left\{ H(t)\frac{dT}{dt} + T(t)\frac{dH}{dt} - T_0(-H)\frac{dH}{dt} \right\} \\ &= \rho_0 C_p \left\{ -H(t)\frac{dT_0}{dz}\frac{dH}{dt} + T_0(-H)\frac{dH}{dt} - T_0(-H)\frac{dH}{dt} \right\} \\ &= -\rho_0 C_p H(t)\frac{dT_0}{dz}\frac{dH}{dt}, \end{aligned} \tag{3.1}$$

where ρ_0 and C_p are the reference density and specific heat of sea water, H_{max} is the total depth of the water column, $Q(t)$ is the surface heat flux ($Q < 0$ for cooling). This leads to a physically intuitive evolution equation for the MLD:

$$\frac{dH^2}{dt} = -\frac{2Q(t)}{\rho_0 C_p}\left(\frac{dT_0}{dz}\right)^{-1}. \tag{3.2}$$

The evolution of the square of MLD is proportional to the rate of heat loss and inversely proportional to the initial stratification. This relationship is only applicable under cooling conditions ($Q < 0$) and increasing H. When the water column is heated the stratification develops at the surface and this simple model cannot represent the sudden shoaling of MLD.

3.2.2 Evolution of of the oxygen flux

Next we apply similar principle to the evolution of dissolved oxygen. The diffusive oxygen gas flux is parameterized as the product of gas transfer velocity (G) and the air-sea disequilibrium of oxygen ($\delta O_2 = [O_2] - [O_{2,sat}]$). The bubble injection flux (F_{inj}) is treated as a positive constant term. The total surface oxygen flux is the sum of diffusive and bubble mediated fluxes, so that

$$F = -G\delta O_2(t) + F_{inj}, \tag{3.3}$$

where $\delta O_2(t) = O_2(t) - O_{2,sat}(T(t))$ is the oxygen saturation state in the mixed layer. We first consider the oxygen budget of the water column where air-sea oxygen flux is balanced by the changes in the oxygen content.

$$\begin{aligned} F &= \frac{d}{dt}\left\{ O_2(t)H(t) + \int_{-H_{max}}^{-H(t)} O_{2,0}(z)dz \right\} \\ &= H(t)\frac{dO_2}{dt} + O_2(t)\frac{dH}{dt} - O_{2,0}(-H)\frac{dH}{dt}, \end{aligned} \tag{3.4}$$

where $O_{2,0}(z)$ is the initial O_2 profile. The first term in the RHS of Eq.3.4 is the change in the mixed layer O_2 content, and the second and third term are the entrainment of subsurface O_2 from below the mixed layer. This model is relevant to the winter-time condition, and the biological O_2 consumption is omitted, however, it implicitly represents the biological effects through the relative depletion of subsurface O_2. When the entrainment mixes subsurface O_2 into the surface layer, it can cause undersaturation of the surface water.

The oxygen budget can then be transformed into the budget equation for the oxygen saturation, $\delta O_2(t)$. Eq.3.1 and 3.4 can be combined with the temperature dependence of oxygen solubility where $A = \frac{dO_{2,sat}}{dT}$:

$$H(t)\frac{d\delta O_2}{dt} = -\left\{\delta O_2 - \delta O_{2,0}(-H)\right\}\frac{dH}{dt} + F - \frac{A\,Q(t)}{\rho_0 C_p}. \tag{3.5}$$

The LHS is the oxygen saturation change in the mixed layer. The first term on the RHS is the entrainment of subsurface δO_2, the second term is the air-sea O_2 flux, and the third term is the solubility change due to the air-sea heat flux.

Given the initial profile of T and O_2, we can calculate the initial profile of δO_2. This equation can be numerically integrated using Eq. 3.2 forced by the air-sea heat flux, Q. Also, under certain limit case scenario, the analytical solutions can be obtained, providing some insight into the system behavior.

3.2.3 Case 1: weak entrainment

First, we explore the limit case scenario where Eq.3.5 is dominated by the diffusive gas exchange. Here we assume that the deepening of mixed layer is relatively slow compare to the air-sea equilibration of diffusive gas transfer, so $\delta O_2 \sim 0$. The total heat loss equals the heat content change in the mixed layer, which is linked to the deepening of MLD:

$$\int_0^t Q(t')dt' = \rho_0 C_p \left\{ T_0(-H)H(t) - \int_{-H(t)}^0 T_0(z)dz \right\}. \tag{3.6}$$

The total oxygen uptake is equal to the change of δO_2 ($\delta O_2 = 0$ in the mixed layer at the end of each time step in this case) plus the change due to the cooling-induced solubility increase.

$$\int_0^t F(t')dt' = -\int_{-H(t)}^0 \delta O_{2,0}(z)dz + A\frac{\int_0^t Qdt}{\rho_0 C_p}. \tag{3.7}$$

The O_2-OHC ratio for this convective event is

$$\frac{\int_0^t Fdt}{\int_0^t Qdt} = \frac{1}{\rho_0 C_p}\left\{ \frac{-\int_{-H(t)}^0 \delta O_{2,0}(z)dz}{T_0(-H)H - \int_{-H(t)}^0 T_0(z)dz} + A \right\}. \tag{3.8}$$

The first term represents DO enrichment in the mixed layer, and is determined by the initial temperature and δO_2 profiles. The second term is the solubility effect. If we further simplify the problem by assuming that these profiles are linear, then,

$$\frac{\int_0^t Fdt}{\int_0^t Qdt} = -\frac{1}{\rho_0 C_p}\left(\frac{k_{\delta O2}}{k_T} - A \right), \tag{3.9}$$

where $k_{\delta O2}$ and k_T are the vertical gradient of $\delta O_{2,0}(z)$ (assuming $\delta O_{2,0}(0) = \frac{F_{inj}}{G}$) and $T_0(z)$. Usually potential temperature and δO_2 both decrease from the surface towards the bottom, which means $\frac{k_{\delta O2}}{k_T} > 0$, and $A < 0$, so $\frac{\int_0^t Fdt}{\int_0^t Qdt} < 0$. In this limit case scenario, the O_2-OHC ratio is independent of the strength of the surface heat flux as long as the convective mixing is relatively weak and surface waters remain well equilibrated. The O_2-

OHC ratio depends on the relative strength between vertical gradient of δO_2 and potential temperature, $\frac{k_{\delta O2}}{k_T}$. Larger $\frac{k_{\delta O2}}{k_T}$ means that the entrainment of δO_2 is stronger, leading to more oxygen uptake from the atmosphere, for the same amount of heat loss. The vertical gradient of δO_2 is a preconditioning factor, regulating how much undersaturation can potentially occur if the stratified water column is distablized. This hypothetical case, the weak entrainment limit, is a case-limit scenario because the relatively slow entrainment ensures that diffusive gas exchange can fully supply O_2 to bring the surface water to equilibrium. In this case, the entrainment flux of negative δO_2 is fully compensated by the air-sea gas flux, resulting in the largest O_2-OHC ratio. While this is an abiotic model, the biological O_2 consumption is a crucial factor determining the vertical gradient δO_2 ($\delta O_2 = -AOU$, AOU: apparent oxygen utilization). Stronger biological activity leads to a stronger vertical gradient of δO_2 and a larger O_2-OHC ratio.

The real O_2-OHC ratio will be smaller than this extreme case since DO is likely to be always under-saturated during the convective events. Also, in this weak entrainment limit, adding the bubble injection flux does not impact on the O_2-OHC ratio. The total oxygen flux is assumed to be always sufficient enough to to saturate oxygen at the surface. Any additional flux of the bubble mediated processes will result in increased de-gassing by the diffusive fluxes.

3.2.4 Case 2: Strong entrainment

Next we consider the other limit-case scenario in which δO_2 is dominated by the entrainment of subsurface water, and the effect of air-sea gas exchange does not affect the mixed layer δO_2. In this limit, the integral δO_2 balance is set by the entrainment of subsurface waters and the cooling-induced solubility increase.

$$\delta O_2 H(t) - \int_{-H}^{0} \delta O_{2,0}(z) dz = -\frac{A}{\rho_0 C_p} \int_0^t Q(t') dt'. \tag{3.10}$$

This equation can be used to diagnose the air-sea O_2 flux and its relationship to the heat flux. First δO_2 is diagnosed from Eq.3.10 driven by the cooling and the deepening of mixed layer. Then, the diagnosed δO_2 can be used to determine the air-sea O_2 flux through Eq.3.3.

$$F(t) = -\frac{G}{H(t)} \left\{ \int_{-H(t)}^{0} \delta O_{2,0}(z) dz - \frac{A}{\rho_0 C_p} \int_0^t Q(t') dt' \right\} + F_{inj} \tag{3.11}$$

The first term on the RHS means that the convective mixing vertically homogenizes the δO_2 over the mixed layer, and it drives the diffusive air-sea O_2 flux into the ocean. The second term (within the curly bracket) reflects the additional diffusive O_2 uptake due to the solubility increase under intense cooling. The third term is the additional oxygen uptake by the bubble mediated gas flux.

A simple solution can be obtained by assuming linear initial profiles and that constant heat flux $Q(t)$. Eq. 3.2 can be solved for H(t) finding that:

$$H(t) = \sqrt{\frac{-2\,Q\,t}{\rho_0\,C_p\,k_T}}. \tag{3.12}$$

Combining Eq.3.11 and 3.12 yields a theoretical prediction for the O_2-OHC ratio:

$$\frac{\int_0^t F dt}{\int_0^t Q dt} = -\frac{\sqrt{2}G}{3} \left(\frac{-k_T\,t}{\rho_0\,C_p\,Q} \right)^{1/2} \left(\frac{k_{\delta O_2}}{k_T} - A \right) + \frac{F_{inj}}{Q}. \tag{3.13}$$

Similar to the weak entrainment assumption, $\frac{\int_0^t F dt}{\int_0^t Q dt}$ is always negative given that $\frac{k_{\delta O2}}{k_T} > 0$. For the diffusive gas exchange part (first term of Eq. 3.13), the O_2-OHC ratio is related to how the cooling is applied. For a given length of the cooling period, the O_2-OHC ratio is larger when the cooling is less intense. For a fixed amount of heat loss, the O_2-OHC ratio is larger when the cooling is applied over a longer period. Here, the O_2-OHC ratio also depends on the initial gradient of δO_2 and potential temperature, but the relation is more complicated compared to the weak entrainment limit. For this case, the diffusive flux is determined by the δO_2 value in the mixed layer after entrainment from below. $\frac{k_{\delta O2}}{k_T}$

controls how much the δO_2 of the whole mixed layer will decrease for a given heat loss, but the MLD can also affect the averaged δO_2 in the mixed layer. For the same amount of entrainment, δO_2 will decrease more in a shallow mixed layer than in a deep one.

We name this scenario strong entrainment limit. The effect of strong mixing prevents the full air-sea equilibration of O_2 in the mixed layer. In this case, the resulting O_2-OHC ratio is modulated by the kinetics of air-sea gas transfer including the effect of bubbles. This situation again represents an upper limit to the real O_2-OHC ratio since the diffusive flux will be reduced once the surface O_2 concentration increases due to the surface uptake, which is not included in this theoretical calculation. The bubble injection increases the O_2-OHC ratio by introducing additional gas flux that is not directly related to the surface heat flux. The compensation between bubble injection and diffusive exchange is not included since the oxygen increase due to the surface oxygen flux is neglected.

3.2.5 Hypotheses

Building on these theoretical development we hypothesize the three independent factors that determine the O_2-Temperature ratio.

- Temperature sensitivity of O_2 solubility, $A = \partial O_{2,sat}/\partial T$.
- Stratification of temperature and oxygen saturation, $k_{\delta O_2}/k_T$.
- Bubble to heat flux ratio, $\rho_0 \, C_p \, F_{inj}/Q$.

For the typical magnitude of these parameters, these three terms are of the same order of magnitude. The weak entrainment limit of Eq.3.9 is the full expression of the first two mechanisms ($k_{\delta O_2}/k_T - A$). The strong entrainment limit of Eq.3.13 reflects the same mechanisms limited by the finite gas exchange rates and the additional bubble contribution.

Figure 3.3 shows the behavior of the numerical solution of the 1-D convective adjustment model under different surface cooling rates. Here the model is integrated from a linear profile of $T_0(z)$ and $\delta O_{2,0}(z)$ with $k_T = 1 \times 10^{-3} \, ^oC \, m^{-1}$ and $k_{\delta O2} = 4 \times 10^{-2} mmol \, m^{-4}$.

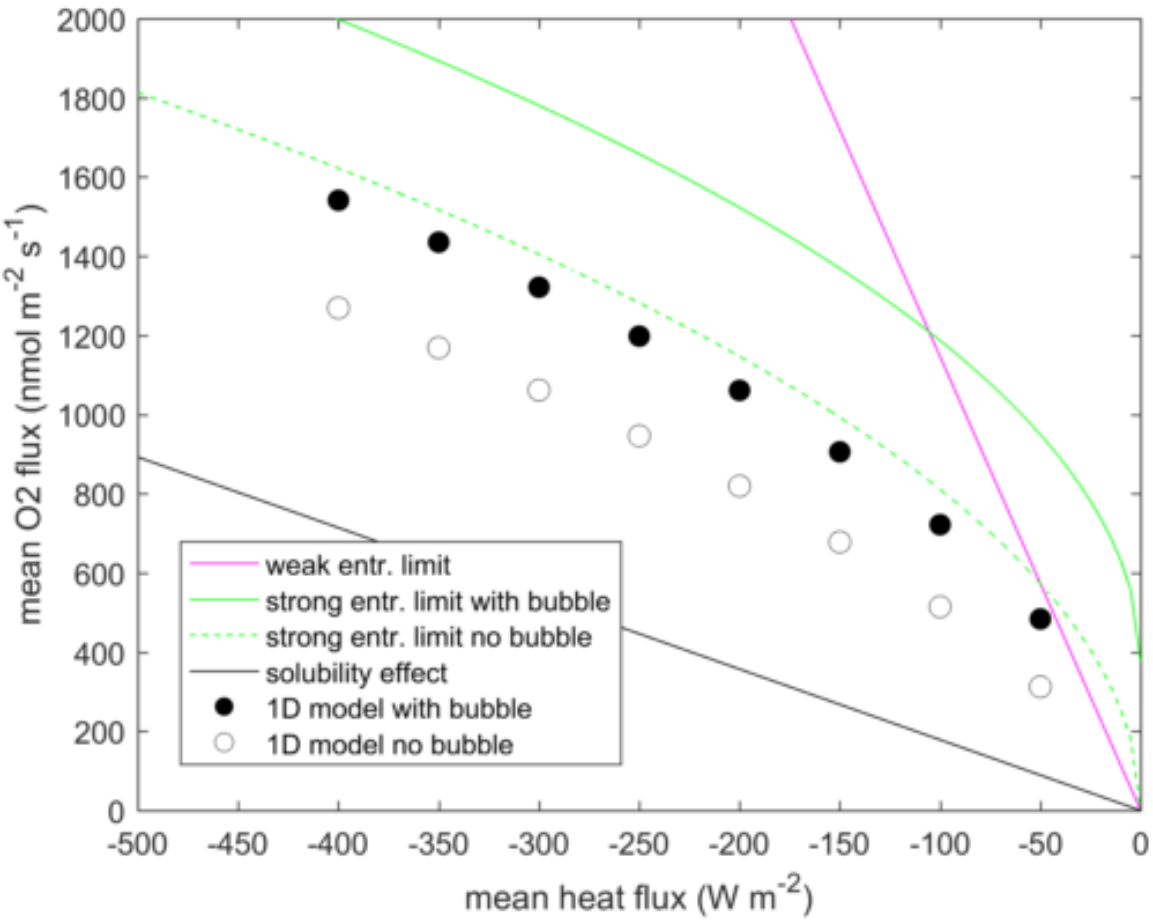

Figure 3.3: Numerical solution of the 1-D convective adjustment model under different cooling rates and for different extreme cases. See text for the parameters of the 1-D convective adjustment model.

We also use a constant gas transfer velocity $G = 1.45 \times 10^{-4} m\, s^{-1}$ and a bubble injection flux $F_{inj} = 3.76 \times 10^{-4} mmol\, m^{-2}\, s^{-1}$.

Numerical solutions of Eq. 3.2 and Eq. 3.5 fall within the region defined by the strong entrainment limit and the solubility effect, $A/(\rho_0\, C_p)$, which represents the change in oxygen solubility due to cooling.

In this framework, there are two definitions of the O_2-OHC ratio. The first type is the O_2-OHC ratio of a single convective event as represented by Eq.3.9 and 3.13. This directly measures the ratio between the time-integrated heat and O_2 fluxes. It would be equivalent of picking a point in Fig 3.3 and calculating y/x. The second type is the interannual change in the O_2-OHC ratio among different winters. For example, December-January-February

(DJF) mean heat and O_2 fluxes can be recorded from a model simulation each year. These winter-time fluxes can vary interannually, with some years having stronger cooling and more O_2 gain. Interannual O_2-OHC ratio can be calculated as a regression coefficient, or a local slope, in Fig 3.3.

In Fig 3.3, the solution shows the negative relationship between loss of heat and gain of oxygen. Stronger heat loss leads to an increase in oxygen uptake. The weak entrainment limit exhibits a strong linear relationship between heat and oxygen fluxes, but it is unlikely relevant to winter-time convection. In this case, the two types of O_2-OHC ratio are identical. When the cooling is strong, as commonly verified during convective events, the behavior of the oxygen uptake is constrained by the strong entrainment limit because the near surface DO remains be under-saturated due to the mixing of deep water to the surface layer. The sensitivity of net oxygen flux to the addition of bubble injection is slightly smaller than the theoretical prediction (F_{inj}/Q), but it is expected due to the partial compensation between diffusive flux and the bubble injection (*Sun et al.*, 2017).

In more realistic conditions, the diffusive flux is reduced because of the elevated surface DO level, which leads to a smaller difference between including or neglecting bubble injection in the calculations (Figure 3.3). The bubble injection contribution to the total flux is greater when the cooling is stronger, which is consistent with the *Sun et al.* (2017). However, when extreme cooling is applied for a very short period, the oxygen uptake can be smaller than that predicted by the solubility effect alone.. This situation is very rare in the real world, and we will further discuss this extreme case in Section 3.4.

3.3 Model hierarchy and experimental design

The theory predicted a range of O_2-OHC ratio in the context of a vertical 1-D water column model under intense cooling and convective mixing. In addition to the temperature-solubility relationship, the theory accounts for the effects of vertical gradients of O_2 and temperature, incomplete air-sea gas exchange and the effect of bubble mediate gas fluxes.

In order to evaluate the theoretical prediction, we simulate directly ocean convection and air-sea gas transfer using a hierarchy of models. We compare the solutions of the 1-D convective adjustment model integrated numerically under different conditions with outputs from:

- a non-hydrostatic simulation of deep convection
- a regional three-dimensional (3-D) simulation of Labrador Sea convection

The vertical 1-D model represents the simplest possible set-up. At the next level, we use a non-hydrostatic model to directly simulate the deep convection in an idealized doubly periodic domain and calculates the vertical exchange of oxygen in the convective plumes. These two models are abiotic, and are applicable only to the winter season. Finally, we use a regional 3-D model of ocean circulation and biogeochemistry configured for the Labrador Sea. This model includes realistic ocean bathymetry, ecosystem and biogeochemical parameterizations, and open lateral boundary conditions. It is computationally expensive, but is realistic, and its output can be directly compared to the available observations.

3.3.1 Non-hydrostatic simulations

We first evaluate the theoretical prediction against a set of sensitivity simulations presented in *Sun et al.* (2017) and performed using the Massachusetts Institute of Technology General Circulation Model (MITgcm) (*Marshall et al.*, 1997a,b). These simulations allow non-hydrostatic dynamics to explicitly resolve deep convection, and the set-up is modified from *Jones and Marshall* (1993).

The model domain is a 32 km $\times$ 32 km box with periodic boundary conditions and horizontal resolution of 250 m. The depth of the water column is 2 km with 41 z-levels whose thicknesses increases from 10 m at surface to 100 m near the bottom. Cooling is applied at the surface with the same amount of total heat loss distributed over events of different duration, and the surface wind speed is fixed (Table 3.1). Diffusive oxygen flux is

Table 3.1: Parameters used for the non-hydrostatic sensitivity experiments. The total heat loss in all experiments is kept the same. The 10 m wind speed is used only for the purpose of calculating the gas transfer coefficient (G) and the bubble-mediated gas flux (F_{inj}). These runs are a subset of the simulations in *Sun et al.* (2017).

Run	period ($days$)	-Q ($W\ m^{-2}$)	$\lvert u_{10}\rvert$ ($m\ s^{-1}$)	Bubble
$c06w15$	6	4000	15	No
$c06w15B$	6	4000	15	Yes
$c15w15$	15	1600	15	No
$c15w15B$	15	1600	15	Yes
$c30w15$	30	800	15	No
$c30w15B$	30	800	15	Yes
$c60w15$	60	400	15	No
$c60w15B$	60	400	15	Yes

applied in all 8 cases, and bubble injection is included in 4 of them. By sampling a wide range of cooling rates from 400 to 4,000 W/m^2, these calculations explore the different responses of entrainment and air-sea equilibration.

In this simulation the model transports oxygen which is influenced by the air-sea gas transfer only. The effect of the biological pump is not directly simulated, and we focus only on the effect of on the effect of winter-time convection. The effect of biology is implicitly included in the initial condition. As the model is initialized in fall (October), the initial vertical gradient of O_2 reflects the summer-time productivity and respiration in the interior ocean. Further details on the set-up can be found in *Sun et al.* (2017).

3.3.2 Regional simulations

To further test our theoretical prediction, we also design a set of regional numerical simulations with the MITgcm. The model domain covers the Labrador Sea (Figure 3.4) with 7.5 km horizontal resolution and 40 vertical layers ranging from 6.25 m (surface) to 250 m (near bottom). The K-profile parameterization (KPP) (*Large et al.*, 1994) is used for vertical mixing, and an ecosystem model with 6 species of phytoplankton and 2 species of zooplankton is included in the simulation (*Pham and Ito*, 2019). Both the diffusive flux and the bubble injection are included for the air-sea oxygen exchange. At the surface the

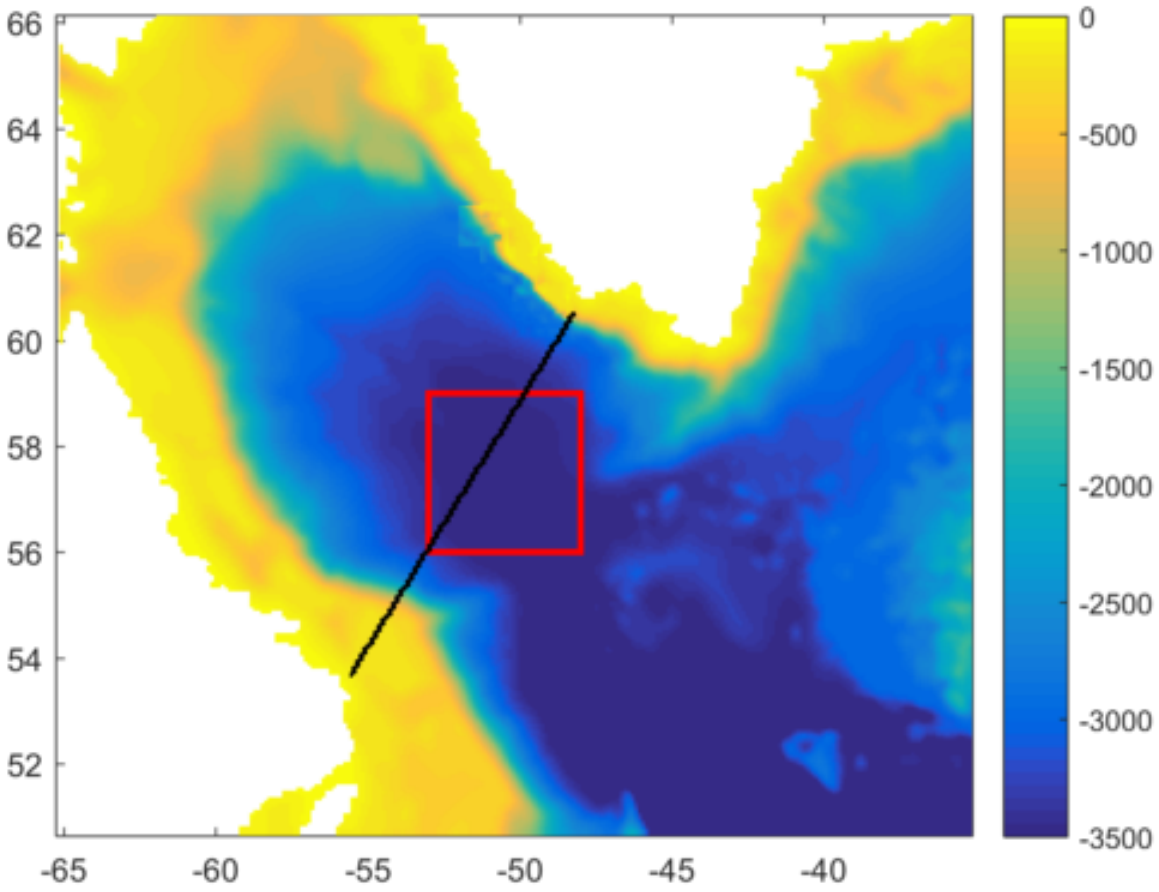

Figure 3.4: Topography of the simulated domain in the Labrador Sea. The black line indicates the WOCE Line AR7W. The red box shows the CLS region defined in this work.

model is forced by the atmospheric reanalysis product based on ERA-Interim (*Dee et al.*, 2011) and uses bulk formula. The physical open boundary conditions are interpolated from the Simple Ocean Data Assimilation ocean/sea ice reanalysis (SODA) 3.4.2 (*Carton et al.*, 2018), , while boundary conditions of phosphate, nitrate, silicate and oxygen are provided by the World Ocean Atlas (WOA18) (*Garcia et al.*, 2018a,b). The boundary conditions for the remaining biogeochemical tracers are derived from the annual cycle produced in the global simulation described in *Pham and Ito* (2019). The parameterization of surface diffusive and bubble injection oxygen flux follows *Sun et al.* (2017).

A set of 4 sensitivity runs is performed over the 8 year period from 2000 to 2007 (Table 3.2). Figure 3.5 compares the simulated potential density ($\sigma - \theta$) and DO with those based on the cruise measurements along the World Ocean Circulation Experiment (WOCE) Line

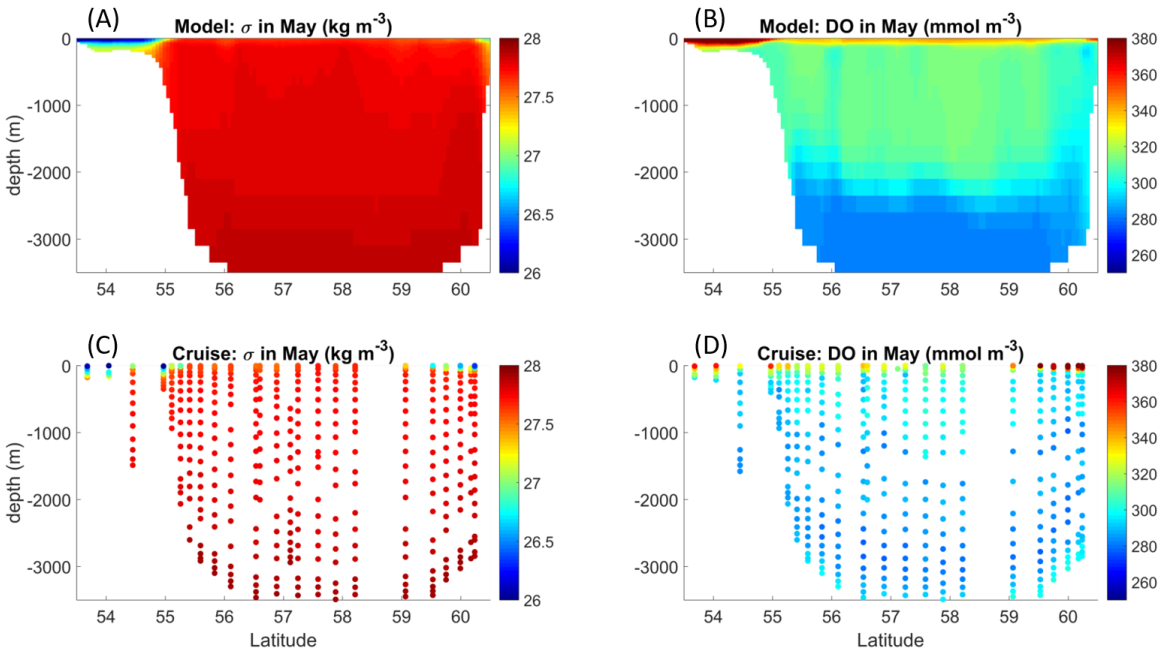

Figure 3.5: Comparison of the model simulated σ (A) and DO (B) and the cruise measurements (CD) along the WOCE Line AR7W in May, 2000.

Table 3.2: Differences between the 4 sensitivity experiments of the Labrador Sea simulation

Run	Reduced cooling	Bubble injection
$CTRL$	No	No
$CTRLB$	No	Yes
$lessC$	Yes	No
$lessCB$	Yes	Yes

AR7W in May, 2000. This hydrography cuts across the deep convective region of the Central Labrador Sea (CLS). Here we define the CLS region defined as the region over (56 ^{o}N - 59 ^{o}N and 53 ^{o}W - 48 ^{o}W) following *Brandt et al.* (2004) and *Luo et al.* (2011). The model shows reasonable skill at simulating the stratification and DO distribution in the Labrador Sea.

The sensitivity experiments are performed modifying the surface boundary conditions. In the $CTRL$ and $lessC$ runs, only the diffusive oxygen flux is applied. The bubble injection flux is added in the $CTRLB$ and $lessCB$ experiments. In $lessC$ and $lessCB$ runs, the winter time (DJF) heat loss is reduced compared to the reanalysis data in the CLS region. The reduced cooling is applied as a Gaussian function peaking at the center of the CLS.

3.4 Results

Sun et al. (2017) examined the effect of bubble injection to the net air-sea oxygen flux in the context of an idealized, non-hydrostatic model. Briefly, the effect of bubble flux was found to be negligible when the water column is well stratified. This is consistent with the weak entrainment limit in section 3.2.3. The additional oxygen input from the bubble flux only raises the surface DO concentration which drives the diffusive outgassing to cancel out the bubble flux, thus there is no net change to the air-sea oxygen transfer. The bubble flux has the largest impact during the cool seasons when convection occurs. The intense mixing maintains undersaturated DO at the ocean surface and and both diffusive and bubble-mediated gas flux can bring oxygen into the ocean. This is consistent with the strong entrainment limit described in section 3.2.4. The next sections focus on the regional 3-D simulations of the Labrador Sea and on understanding the mechanisms that control the O_2-OHC ratio.

3.4.1 The bubble effect

In *Sun et al.* (2017) the model was integrated only for the cool season, focusing on the effect of deep convection. With the regional model, we can now address the full seasonal cycle as well as interannual variability. Figure 3.6A shows the multi-year time series of air-sea oxygen flux over the CLS region (positive into the ocean). The majority of oxygen uptake takes place in winter since the wind is stronger at this time of the year and DO is close to saturation or supersaturation in the warmer seasons. There are four lines in this diagram. Blue curves are from the $CTRL$ (solid) and $CTRLB$ (dash), that differ only for the presence of the bubble injection flux in the $CTRLB$ case. Red curves are from the $lessC$ (solid) and $lessCB$ (dash), in which cooling is reduced over the CLS region. The winter-time oxygen uptake weakens when the cooling rate is reduced, and the change in oxygen flux is much larger than what expected from the change of oxygen solubility (Figure

3.6B). This indicates that the oxygen flux decreases primarily because of less entrainment of the under-saturated deep water.

Consistently with *Sun et al.* (2017), adding the bubble injection has the largest impact on the net air-sea oxygen transfer in winter. This is due to two reasons. Firstly, F_{inj} is stronger in winter due to the strong surface winds. Secondly, in the warm seasons the bubble injection flux is mostly compensated. When bubble injection is added, the DO concentration increases in the surface, and this pushes the surface DO towards saturation or super-saturation, thus reducing the diffusive flux. The response of surface DO is fast when the MLD is shallow in the warm seasons. In this stratified condition, the entrainment of the undersaturated water from deeper layers is weak. The compensation between the bubble injection and the diffusive flux is weaker when the vertical mixing is stronger, which leads to larger increase in DO by adding bubble injection. By the same argument, adding bubble injection in the reduced cooling cases ($lessC$ and $lessCB$) has a lesser impact.

Figure 3.7 shows the spatial pattern of air-sea oxygen flux and its breakdown in a typical winter (January, 2003). The compensation is clearly visible in the difference between $CTRL$ and $CTRLB$ runs (Fig 3.7BC) even in the cool season. The change in the diffusive oxygen fluxes between the two runs (Fig 3.7d) indicates that there is a significant compensation. The changes in diffusive flux have similar patterns to the bubble injection flux but opposite sign, but the compensation is not complete, and it causes a net increase of oxygen uptake. Considering the winter (DJF) mean oxygen flux over the CLS, 79% of the bubble injection flux is compensated by the reduction of diffusive flux in $CTRLB$ run, while the compensation rate is 87% in $lessCB$ run. In *Sun et al.* (2017) the compensation rate was predicted to be larger for weaker vertical mixing, and was found to be 65.8% for the case with the weakest cooling of 400 W m^{-2} at surface, In our regional simulations, the DJF mean surface heat flux is even weaker (about -200 W m^{-2} for $CTRL$ and $CTRLB$ and -120 m^{-2} for $lessC$ and $lessCB$), which is consistent with a larger compensation rate.

To summarize, the winter time oxygen uptake largely depends on the surface cool-

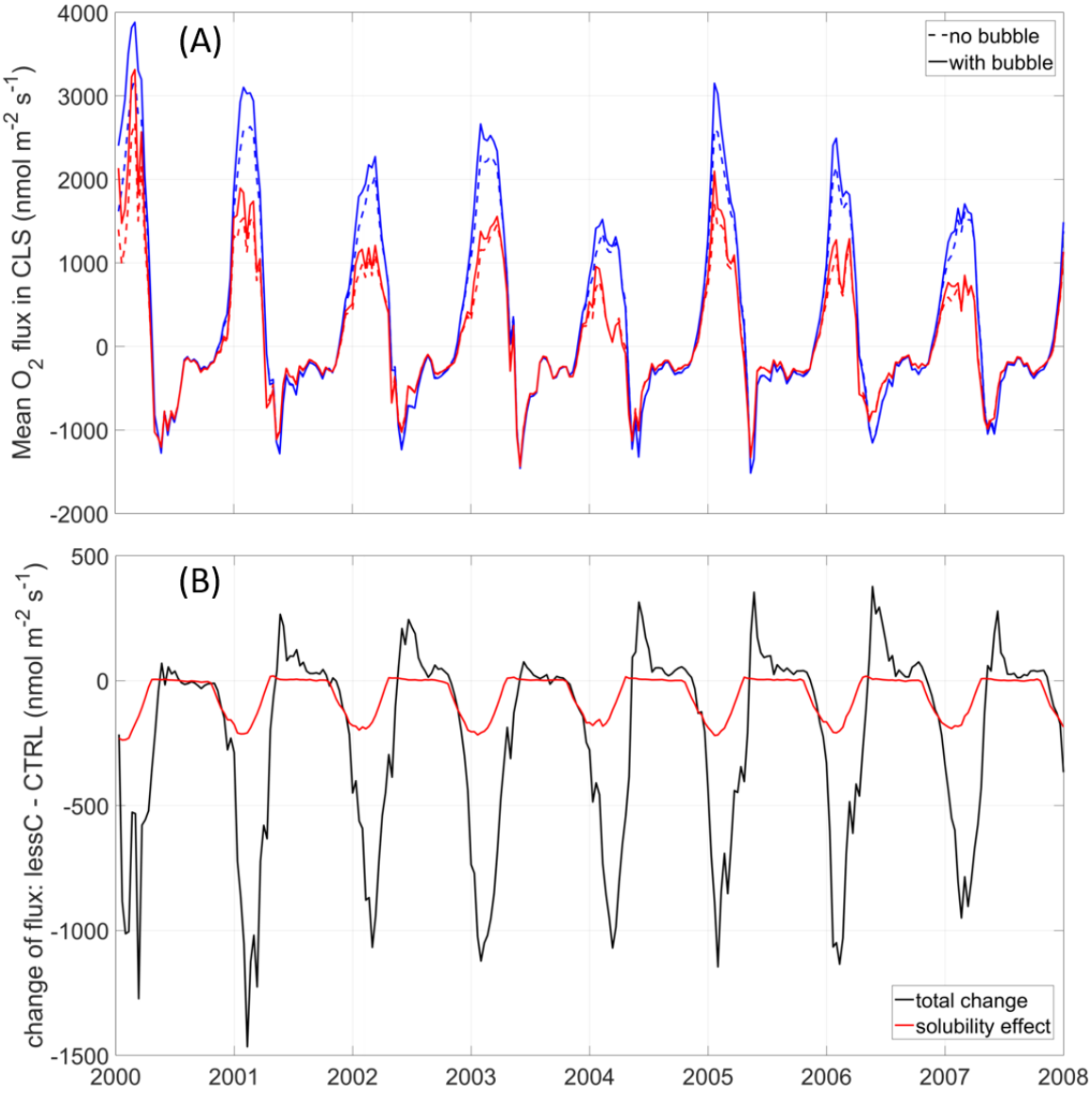

Figure 3.6: (A)Mean total surface oxygen flux in the CLS. The dashed curves indicate results of cases without bubble injection ($CTRL$ and $lessC$), while the solid curves are the results of cases with bubble injection ($CTRLB$ and $lessCB$). The blue curves show the outcome from $CTRL$ and $CTRLB$, and the red curves from the runs with reduced reduced winter cooling ($lessC$ and $lessCB$). (B)The difference in surface oxygen flux between $lessC$ and $CTRL$ (black) and the contribution due to the solubility change (red).

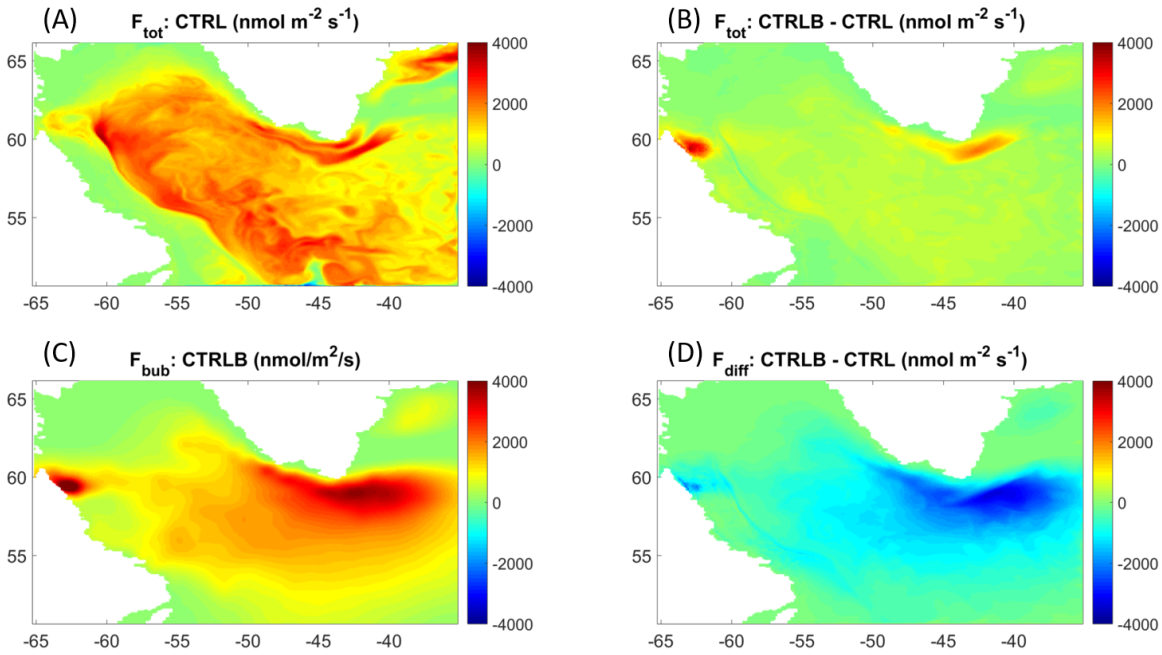

Figure 3.7: (A) Mean surface oxygen flux in $CTRL$ in Jan, 2003. (B) Difference total flux between $CTRLB$ and $CTRL$. (C) Bubble injection effect in $CTRLB$ (bottom left). (D) Change in diffusive flux between $CTRLB$ and $CTRL$.

ing. The enlarged entrainment of subsurface water is likely to be the main reason of the strengthening of oxygen uptake under stronger cooling. Bubble injection brings additional oxygen into the ocean, but a large portion of it is compensated by the reduced diffusive flux. The compensation is stronger when the cooling is weaker. Here we focus only on the mean strength of the cooling, but, as suggested by *Sun et al.* (2017), also the duration of the cooling affects largely the oxygen flux during the convective events. We further address the effect of different cooling durations next.

3.4.2 The effect of atmospheric forcing

Here we test the theoretical predictions of the O_2-OHC ratio in the strong entrainment limit (Eq.3.13) using the non-hydrostatic simulations. The theory predicts that the magnitude of the O_2-OHC ratio increases with time under constant cooling. The non-hydrostatic simulations are consistent with the numerical integration of the 1-D model and the strong entrainment limit prediction (Fig 3.8).

In Figure 3.8 each dot represents the results of a numerical simulation. As the cooling duration increases, the magnitude of cooling (Q) decreases so that the total heat loss remains the same for all cases. When the total heat loss is fixed, the O_2-OHC ratio is larger in magnitude when the cooling is applied over a longer period with a linear relationship (since $Q \propto t^{-1}$). The model output deviates from the predicted linear relationship due to the effect of the surface oxygen flux on the DO concentration. This effect becomes more significant when the cooling is less intense and the cooling period is longer.

In our model configuration, the surface flux can be extremely strong when the cooling period is short, which makes the O_2-OHC ratio even smaller than the solubility effect. In this limit, the bottleneck is the finite gas exchange timescale of the air-sea oxygen flux. For a cooling time of $\sim$20 days or shorter, there is not enough time for the surface water DO concentration to respond to the increased air-sea flux. Under these extreme conditions, the solubility increase due to the cooling is faster than the increase of DO due to the surface oxygen flux in the MLD. In the high latitude regions, the cool season lasts for several months, so a very small O_2-OHC ratio is unlikely.

As the cooling period gets longer, the amplitude of the O_2-OHC ratio increases. The theoretical magnitude of the O_2-OHC ratio is always greater than the numerical model outputs, as expected. The results from the vertical 1-D model and the non-hydrostatic model are similar, but the non-hydrostatic model shows a slightly larger magnitude of the O_2-OHC ratio with $\sim$-2.5 $nmolO_2/J$ for 30 days of cooling, which is close to the temperature-solubility relationship. For 60 days of cooling, magnitude increases significantly reaching about -4.0 $nmolO_2/J$. In reality, the cool period can last longer than 60 days, so the amplitude of the O_2-OHC ratio can be greater than -4.0 $nmolO_2/J$ depending on the length and intensity of the heat loss.

This demonstrates the complexity of the factors controlling the O_2-OHC ratio, as changes in atmospheric forcing can be conductive to very different outcomes.

3.4.3 Interannual variability of the O_2-OHC ratio

Given the importance of the atmospheric forcing, we examine in more detail the regional, 3-D simulations of the Labrador Sea forced with the atmospheric reanalysis data. Unlike the vertical 1-D and non-hydrostatic model, this model uses realistic boundary conditions and simulates the full seasonal cycle. Figure 3.9 shows the mean surface oxygen flux (F) as a function of the mean cooling rate Q over the winter months (DJF) over the seven years from 2001 to 2007.

Each dot represents the winter oxygen and heat fluxes for the 7 years. Open blue circles are for the $CTRL$ run, and the filled blue circles for the $CTRLB$ run. Open red circles represent the $lessC$ run, and the filled red circles the $lessCB$ run.

Our theory is based on the linear stratification of T and δO_2. Here, k_T and $k_{\delta O2}$, used in the calculation of the weak entrainment and strong entrainment limits, are the regression coefficients of potential temperature and δO_2 in early December calculated as a function of depth in the $CTRL$ run. Also our theory is based on constant gas transfer velocity, G. The 3-D model parameterizes G based on the daily atmospheric winds. In order to make a comparison with the theory, a representative G is estimated from the regression of winter time oxygen diffusive flux and surface δO_2. The duration of the event is set to be 3 month as DJF is investigated here.

The outcome of the 3-D simulation is bounded by the theoretical predictions for the solubility effect (black) and the strong entrainment limit with bubble effect (solid green). Bubble injection provides additional oxygen flux, and the increment is greater when the cooling is more intense due to the strong entrainment. The oxygen flux mostly lie above the lower boundary defined by the solubility effect alone and below the strong entrainment limit. The weak entrainment limit suggests constant O_2-OHC ratio as shown in Eq.3.9. The strong entrainment limit (green) predicts a non-linear relationship between the heat flux and oxygen flux (Eq.3.13).

The stratification and vertical DO distribution vary among different years, so it is diffi-

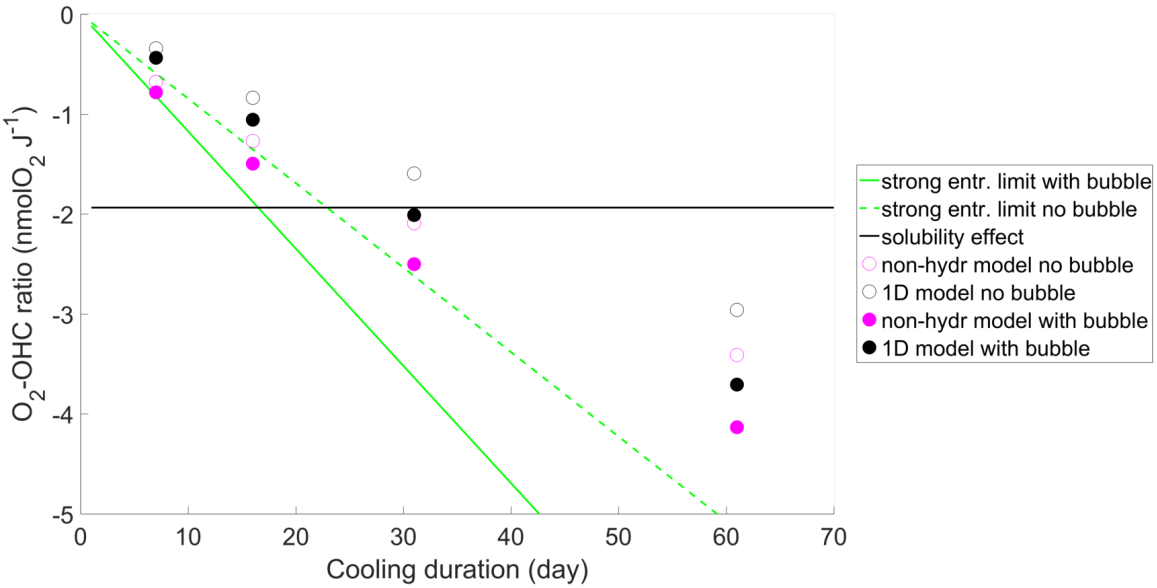

Figure 3.8: The O_2-OHC ratio as a function of cooling duration from the non-hydrstatic simulations compared with the solutions of the 1-D convective adjustment model.

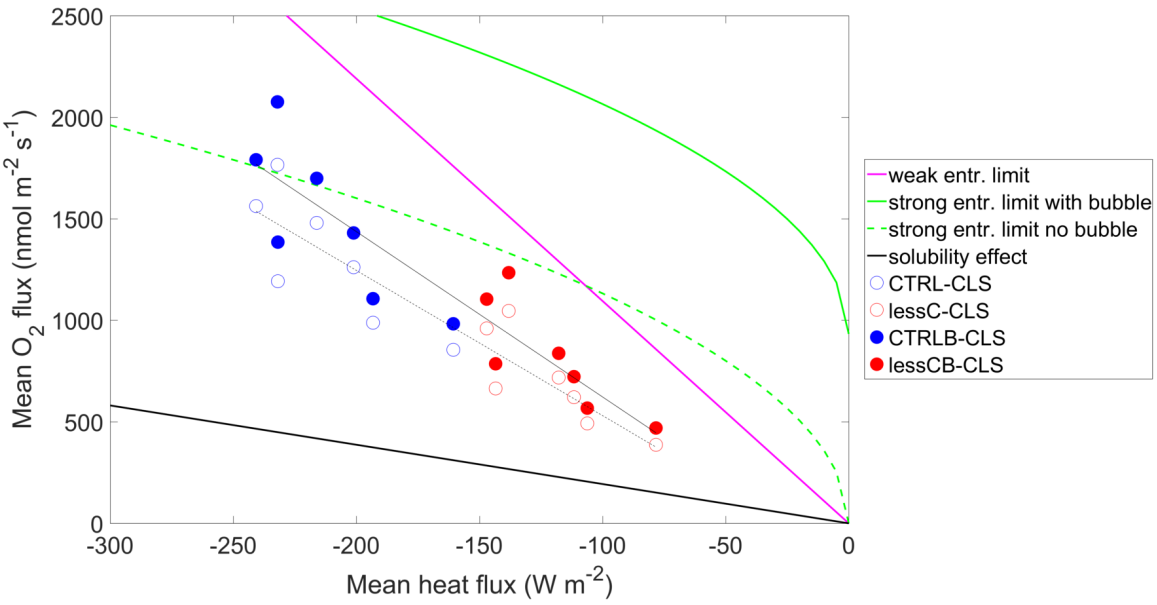

Figure 3.9: Mean air-sea oxygen flux as a function of mean surface heat flux over 7 different winters (from DJF between 2000 and 2001 to DJF between 2006 and 2007) in the CLS from the regional simulations compared with the theoretical predictions under different assumptions.The thin solid black line is the linear fitting for the 16 points with bubble injection ($CTRLB$ and $lessCB$). The thin dashed black line is the linear fitting for the 16 points without bubble injection ($CTRL$ and $lessC$).

cult to make exact comparison with the theory, but Figure 3.9 shows a quasi-linear relationship between the mean rate of cooling and the oxygen uptake in the CLS region. It is also an open domain, and the lateral transport is clearly important for the regional oxygen budget and the evolution of DO concentrations in the mixed layer. In the regional set-up, the stratification is also affected by salinity and by the freshwater fluxes at the ocean surface. All these factors contribute to the O_2-OHC ratio interannual differences.

For predicting the future evolution of the DO inventory, the sensitivity of the total oxygen uptake to changes in heat fluxes is likely most important. This interannual O_2-OHC ratio can be calculated as a regression coefficient of the mean oxygen flux onto the heat flux. Under the weak entrainment limit, the formula for the interannual O_2-OHC ratio is identical to Eq. 3.9,

$$\frac{d\int_0^t F dt}{d\int_0^t Q dt} = -\frac{1}{\rho_0 C_p}(\frac{k_{\delta O2}}{k_T} - A), \tag{3.14}$$

which is independent of the the heat flux strength. Assuming that the cooling duration is constant, under the strong entrainment limit the interannual O_2-OHC ratio can be written as the derivative of 3.13 with respect to $-Qt$:

$$\frac{d\int_0^t F dt}{d(Qt)} = -\frac{G}{3}(\frac{k_T}{2\rho_0 C_p})^{1/2}(\frac{k_{\delta O2}}{k_T} - A)\frac{t}{(-Qt)^{1/2}}. \tag{3.15}$$

This is proportional to $(-Q)^{-1/2}$, indicating a smaller ratio for strong cooling as shown in Fig 3.9. The explicit dependence on the bubble flux, F_{inj}, disappears from the equation.

Another factor to consider is the variability in the initial profiles of temperature and DO among cases and years. For the strong entrainment limit, larger k_T also implies larger ratio for a given $\frac{k_{\delta O2}}{k_T}$. The difference in the interannual O_2-OHC ratio between the cases with bubble injection and those without occurs indirectly through altering the surface δO_2. With all other conditions being the same, the bubble injection flux increases the vertical δO_2 gradient, which makes the magnitude of the interannual O_2-OHC ratio larger (thin solid green line compared to the thin dashed green line in Figure 3.9). Another factor is

Table 3.3: Regression coefficient ($nmolO_2\,J^{-1}$) between the mean surface oxygen flux and heat flux over DJF in 7 different years (2001-2007) in the CLS compared with the theoretical prediction under weak entrainment (Eq. 3.14) and strong entrainment (Eq. 3.15) limits with the mean vertical gradient of potential temperature and δO_2 extrapolated from different regional simulations.

Run	$\frac{d(Ft)}{d(Qt)}$	Eq. 3.9	Eq. 3.15	k_T ($^oC\,m^{-1}$)	$k_{\delta O2}$ ($mmol\,m^{-4}$)
$CTRL$	-9.42	-11.10	-3.90	4.35×10^{-4}	1.65×10^{-2}
$CTRLB$	-11.20	-11.94	-4.19	4.35×10^{-4}	1.80×10^{-2}
$lessC$	-8.04	-10.17	-5.00	4.86×10^{-4}	1.65×10^{-2}
$lessCB$	-9.22	-10.90	-5.36	4.86×10^{-4}	1.80×10^{-2}

the correlation between F_{inj} and Q through the wind speed. Stronger evaporative cooling is often driven by the stronger surface wind speed, which drives stronger F_{inj}. This causes additional sensitivity to the heat flux in $CTRLB$ and $lessCB$ runs. The difference of the interannual O_2-OHC ratio between $CTRL$ (or $CTRLB$) and $lessC$ (or $lessCB$) is more complicated since both the initial vertical gradient and the cooling rate change. Our simulations suggest that the interannual O_2-OHC ratio is larger in $CTRL$ ($CTRLB$) than in $lessC$ ($lessCB$).

Plugging in the mean $k_{\delta O2}$ and k_T estimated from different simulations, the weak entrainment and strong entraiment limits predict the same order of magnitude for the 4 runs. The weak entrainment limit overestimates the ratio, while the strong entrainment limit always predicts ratios that are too low (Table 3.3). Relatively, the weak entrainment limit fits better the behavior of the regional model. A possible explanation is that, even though a few intense convective events may happen during the winter, the relative strength of surface oxygen flux and entrainment may actually be closer to the weak entrainment limit when averaged for the whole 3-month period, at least in the years considered, all characterized by relatively weak convection in the Labrador Sea region (*Luo et al.*, 2014; *Yashayaev and Loder*, 2016).

3.5 Discussion

In this work, we investigated the relation between the surface oxygen flux and the heat flux during deep convection events considering its importance on setting the O_2-OHC ratio in the ocean interior. Based on theoretical predictions and model simulations of different complexity, we find that the O_2-OHC ratio depends on how the cooling is applied. The injection of bubbles can modify this ratio.

On one hand, the surface cooling increases the surface oxygen solubility and leads to larger diffusive oxygen flux. On the other hand, the cooling weakens the stratification of the water column and deepens the MLD, which brings more under-saturated water from the subsurface and further enhances the surface oxygen flux. The total oxygen uptake is larger with stronger cooling. Additionally, the duration of the cooling episodes matters, with longer episodes letting more oxygen into the ocean. When the initial conditions are fixed and only the thermal buoyancy forcing is considered, the O_2-OHC ratio becomes smaller in magnitude under stronger cooling applied for a shorter period. For a single convection event, the oxygen uptake can be insufficient when the cooling is intense or there is not enough time for the ventilation. Adding bubble injection can increase the O_2-OHC ratio, even though part of the bubble injection flux will be compensated by the decreasing diffusive flux due to the elevated surface DO level. The impact of the bubble injection increases under the intense cooling. The variability of O_2-OHC ratio under realistic conditions is more complicated. For example, in our study we assumed that the buoyancy forcing mainly comes from the surface heat flux, but deep convection can also be driven by a strong surface salinity flux. The haline driven convection can potentially lead to very large O_2-OHC ratio because of the entrainment of subsurface water in the absence of strong cooling.

In our regional simulations, the interannual O_2-OHC ratio for the newly formed LSW is -9.42 $nmolO_2\ J^{-1}$ without bubble injection and -11.20 $nmolO_2\ J^{-1}$ with bubble injection.

These values are larger than global estimates from climate ocean models (*Keeling et al.*, 2010; *Ito et al.*, 2017), but in broad agreement with the observational estimate of the O_2-OHC ratio for the North Atlantic Deep Water (NADW) in *Keeling and Garcia* (2002) (7.5 - 10 $nmolO_2\,J^{-1}$). For the interannual variability of the O_2-OHC ratio, the difference in the initial conditions becomes important. The initial vertical gradient of temperature and δO_2 depend on the stratification and the biological pump, respectively. Our regional simulations of the Labrador Sea show lower interannual O_2-OHC ratio when surface cooling is reduced (-9.2 $nmolO_2\,J^{-1}$ in $lessCB$ versus -11.2 $nmolO_2\,J^{-1}$ in $CTRLB$), consistent with the prediction from *Plattner et al.* (2002). Our theory and model suggest that it is likely due to the stronger vertical gradient of potential temperature. In a warming climate, k_T is bound to increase due to the increasing stratification, leading to a decrease in O_2-OHC ratio holding everything else constant. However, over multiple decades, $k_{\delta O2}$ will also increase due to greater oxygen utilization (*Keeling et al.*, 2010; *Ito et al.*, 2017), which compensates the increase of k_T and it may complicate our projection of the O_2-OHC ratio. Furthermore, recent study by *Tagklis et al.* (2020) showed that the slowdown of the Atlantic Meridional Overturning Circulation reduces the basin-scale upper ocean nutrient inventory, moderating the oxygen loss. Such changes in the large-scale nutrient transport can alter the long-term change in the vertical gradient of DO, and affect the O_2-OHC ratio. The overall change in the O_2-OHC ratio will be determined by the competition of changes in k_T and $k_{\delta O2}$. Despite the simplicity of the theoretical model and the extreme assumption, the weak entrainment limit provides a reasonable first order prediction for the interannual O_2-OHC ratio. Changes of the vertical gradients of potential temperature and DO may be important indicators for rate of deoxygenation in a warming climate.

CHAPTER 4
SUMMARY AND DISCUSSION

This dissertation focuses on better understanding the relationship between oxygen uptake and surface forcing during convective events. By closely examining the mechanisms determining DO content at a site of water mass formation, we highlighted several factors that are potentially important to constrain the oxygen levels in the ocean interior and the future deoxygenation under a warmer climate. Here we summaries our main findings and discuss implications for possible future works.

As suggested by previous works (e.g. *Monahan and Torgersen*, 1990; *Asher and Wanninkhof*, 1998; *Hamme and Severinghaus*, 2007), the bubble-mediated flux can enhance oceanic gas uptake, especially for low solubility gases. We implement a bubble injection parameterization for oxygen proportional to the cubic of the surface wind speed (*Asher and Wanninkhof*, 1998) in model simulations. Under typical winter-time wind conditions, the bubble injection flux can have a magnitude comparable to that of the diffusive flux. However, considerable compensation is observed between bubble injection and diffusive fluxes. The bubble injection elevates the surface DO concentration, which reduces the diffusive flux. This compensation is strong when the entrainment of under-saturated subsurface water is weak. In stratified conditions, commonly found in the warm seasons at high latitudes and year-around at low latitudes, the bubble-mediated gas flux only increases the surface DO level towards super-saturation and does not significantly contribute to the net O_2 uptake. When deep ventilation happens, on the other hand, the bubble-mediated flux can significantly increase the net oxygen uptake as the undersaturation can be maintained by the entrainment of subsurface waters. This can alter the preformed oxygen level of water masses, which is important for the correct estimation of the True Oxygen Utilization (*Ito et al.*, 2004; *Broecker and Peng*, 1982). The O_2-OHC ratio of recently formed water masses

can also be affected by bubble injection. The bubble-mediated flux modifies the O_2-OHC ratio not only through introducing additional oxygen during deep mixing events, but also by changing the vertical oxygen gradient.

The oxygen uptake for a ventilation event is closely linked to the surface cooling, especially when the vertical mixing is mainly driven by the thermal buoyancy forcing (e.g. during winter convection in the Labrador Sea). The temperature drop increases the solubility of oxygen, and the buoyancy loss permits the entrainment of under-saturated subsurface water. Both effects benefit the oxygen uptake with the end result that the total oxygen uptake correlates positively with the total heat loss. Our studies suggest that the duration of the cooling is also important even when the total heat loss is the same. A longer duration of convective mixing leads to larger cumulative O_2 uptake. This further complicated the O_2-OHC ratio of water masses as the O_2-OHC ratio can be smaller in magnitude if a given amount of cooling is applied over a short period rather than over a long one.

The initial vertical gradients of potential temperature and oxygen are also important for the oxygen uptake and the O_2-OHC ratio, and this can be termed as "preconditioning". The water column is "preconditioned" before the winter seasons. The stratification and the saturation status of the subsurface water determine the amplitude of the diffusive flux during the convective events for a given cooling. A weakly stratified water column with large AOU in the subsurface can potentially lead to strong oxygen uptake and large amplitude of the O_2-OHC ratio. The relative strength between the gradient of potential temperature and that of oxygen is a key factor determining the interannual O_2-OHC ratio. This implies that the representation of stratification and the biological pump is essential for the correct estimation of the interannual O_2-OHC ratio under a warming climate.

In this dissertation, we focused on the processes determining the DO level at a site of deep water formation. We propose several mechanisms that are potentially important for the oxygen exchange between ocean and atmosphere, but its global importance is still unresolved. Either observational estimates or numerical estimates using ESMs are necessary

for this purpose. The former require data with good temporal and spatial coverage, and the latter also require more measurements to constrain the bubble-mediated gas flux parameterization. For the DO level in the ocean interior, the ocean circulation and biological-driven consumption also play dominant roles. *Tagklis et al.* (2020) show that the DO trends can be of the opposite sign for low and high latitudes in ESMs due to the different tendencies of biological productivity under a warming climate. Aside from the model simulation approach, the continuously evolving machine learning techniques provide new tools that could help understanding and constraining the dominant mechanisms for oceanic DO variability and to achieve better predictions for deoxygenation in a warming climate.

REFERENCES

Asher, W. E., and R. Wanninkhof (1998), The effect of bubble-mediated gas transfer on purposeful dual-gaseous tracer experiments, *Journal of Geophysical Research: Oceans (1978–2012)*, *103*(C5), 10,555–10,560.

Atamanchuk, D., J. Koelling, U. Send, and D. Wallace (2020), Rapid transfer of oxygen to the deep ocean mediated by bubbles, *Nature Geoscience*, pp. 1–6.

Bopp, L., C. Le Quéré, M. Heimann, A. C. Manning, and P. Monfray (2002), Climate-induced oceanic oxygen fluxes: Implications for the contemporary carbon budget, *Global Biogeochem. Cycles*, *16*, 1022, doi:10.1029/2001GB001445.

Bopp, L., L. Resplandy, J. C. Orr, S. C. Doney, J. P. Dunne, M. Gehlen, P. Halloran, C. Heinze, T. Ilyina, R. Séférian, J. Tjiputra, and M. Vichi (2013), Multiple stressors of ocean ecosystems in the 21st century: projections with cmip5 models, *Biogeosciences*, *10*(10), 6225–6245, doi:10.5194/bg-10-6225-2013.

Boyer, T., J. I. Antonov, O. K. Baranova, C. Coleman, H. E. Garcia, A. Grodsky, D. R. Johnson, R. A. Locarnini, A. V. Mishonov, T. D. O'Brien, C. R. Paver, J. R. Reagan, D. Seidov, I. V. Smolyar, and M. M. Zweng (2013), World ocean database 2013, *Report*, NOAA.

Bracco, A., and J. Pedlosky (2003), Vortex generation by topography in locally unstable baroclinic flows, *Journal of Physical Oceanography*, *33*(1), 207–219, doi:10.1175/1520-0485(2003)033⟨0207:vgbtil⟩2.0.co;2.

Brandt, P., F. A. Schott, A. Funk, and C. S. Martins (2004), Seasonal to interannual variability of the eddy field in the labrador sea from satellite altimetry, *Journal of Geophysical Research: Oceans*, *109*(C2).

Broecker, W. S., and T.-H. Peng (1982), *Tracers in the Sea*, Lamont-Doherty Geological Observatory, Columbia University.

Carton, J. A., G. A. Chepurin, and L. Chen (2018), Soda3: a new ocean climate reanalysis, *Journal of Climate*, *31*(17), 6967–6983.

Clarke, R. A., and J. C. Gascard (1983), The formation of labrador sea-water .1. large-scale processes, *Journal of Physical Oceanography*, *13*(10), 1764–1778, doi:10.1175/1520-0485(1983)013⟨1764:tfolsw⟩2.0.co;2.

Codispoti, L. A. (1995), Is the ocean losing nitrate?, *Nature*, *376*(6543), 724.

Dee, D. P., S. M. Uppala, A. J. Simmons, P. Berrisford, P. Poli, S. Kobayashi, U. Andrae, M. A. Balmaseda, G. Balsamo, P. Bauer, P. Bechtold, A. C. M. Beljaars, L. van de Berg, J. Bidlot, N. Bormann, C. Delsol, R. Dragani, M. Fuentes, A. J. Geer, L. Haimberger, S. B. Healy, H. Hersbach, E. V. Holm, L. Isaksen, P. Kallberg, M. Kohler, M. Matricardi, A. P. McNally, B. M. Monge-Sanz, J. J. Morcrette, B. K. Park, C. Peubey, P. de Rosnay, C. Tavolato, J. N. Thepaut, and F. Vitart (2011), The era-interim reanalysis: configuration and performance of the data assimilation system, *Quarterly Journal of the Royal Meteorological Society*, *137*(656), 553–597, doi:10.1002/qj.828.

Falina, A., A. Sarafanov, and A. Sokov (2007), Variability and renewal of labrador sea water in the irminger basin in 1991–2004, *Journal of Geophysical Research: Oceans*, *112*(C1).

Fuchs, G., W. Roether, and P. Schlosser (1987), Excess 3he in the ocean surface layer, *Journal of Geophysical Research: Oceans*, *92*(C6), 6559–6568, doi:10.1029/JC092iC06p06559.

Garcia, H. E., and L. I. Gordon (1992), Oxygen solubility in seawater: Better fitting equations, *Limnology and oceanography*, *37*(6), 1307–1312.

Garcia, H. E., R. A. Locarnini, T. P. Boyer, J. I. Antonov, O. K. Baranova, M. M. Zweng, and D. R. Johnson (2010), World ocean atlas 2009, volume 3: Dissolved oxygen, apparent oxygen utilization, and oxygen saturation., *Report*.

Garcia, H. E., K. Weathers, C. R. Paver, I. Smolyar, T. P. Boyer, R. A. Locarnini, M. M. Zweng, A. V. Mishonov, O. K. Baranova, D. Seidov, and J. R. Reagan (2018a), World ocean atlas 2018, volume 3: Dissolved oxygen, apparent oxygen utilization, and oxygen saturation, *edited by: Mishonov, A., NOAA Atlas NESDIS*, *83*, 38.

Garcia, H. E., K. Weathers, C. R. Paver, I. Smolyar, T. P. Boyer, R. A. Locarnini, M. M. Zweng, A. V. Mishonov, O. K. Baranova, D. Seidov, and J. R. Reagan (2018b), World ocean atlas 2018, volume 4: Dissolved inorganic nutrients (phosphate, nitrate and nitrate+nitrite, silicate), *edited by: Mishonov, A., NOAA Atlas NESDIS*, *84*, 35.

Gascard, J. C., and R. A. Clarke (1983), The formation of labrador sea-water. part ii. mesoscale and smaller-scale processes, *Journal of Physical Oceanography*, *13*(10), 1779–1797, doi:10.1175/1520-0485(1983)013⟨1779:tfolsw⟩2.0.co;2.

Hall, T. M., T. W. N. Haine, M. Holzer, D. A. Lebel, F. Terenzi, and D. W. Waugh (2007), Ventilation rates estimated from tracers in the presence of mixing, *Journal of Physical Oceanography*, *37*(11), 2599–2611, doi:10.1175/2006jpo3471.1.

Hamme, R. C., and S. R. Emerson (2002), Mechanisms controlling the global oceanic distribution of the inert gases argon, nitrogen and neon, *Geophysical Research Letters*, *29*(23), doi:10.1029/2002gl015273.

Hamme, R. C., and S. R. Emerson (2006), Constraining bubble dynamics and mixing with dissolved gases: Implications for productivity measurements by oxygen mass balance, *Journal of Marine Research*, *64*(1), 73–95.

Hamme, R. C., and J. P. Severinghaus (2007), Trace gas disequilibria during deep-water formation, *Deep Sea Research Part I: Oceanographic Research Papers*, *54*(6), 939–950.

Ho, D. T., C. S. Law, M. J. Smith, P. Schlosser, M. Harvey, and P. Hill (2006), Measurements of air-sea gas exchange at high wind speeds in the southern ocean: Implications for global parameterizations, *Geophysical Research Letters*, *33*(16).

Ito, T., M. Follows, and E. Boyle (2004), Is aou a good measure of respiration in the oceans?, *Geophysical research letters*, *31*(17).

Ito, T., R. C. Hamme, and S. Emerson (2011), Temporal and spatial variability of noble gas tracers in the north pacific, *Journal of Geophysical Research: Oceans (1978–2012)*, *116*(C8).

Ito, T., S. Minobe, M. C. Long, and C. Deutsch (2017), Upper ocean o2 trends: 1958–2015, *Geophysical Research Letters*, *44*(9), 4214–4223, doi:10.1002/2017GL073613, 2017GL073613.

Jenkins, W. (1988), The use of anthropogenic tritium and helium-3 to study subtropical gyre ventilation and circulation, *Philosophical Transactions of the Royal Society of London. Series A, Mathematical and Physical Sciences*, *325*(1583), 43–61.

Johnson, G. C., S. Schmidtko, and J. M. Lyman (2012), Relative contributions of temperature and salinity to seasonal mixed layer density changes and horizontal density gradients, *Journal of Geophysical Research: Oceans*, *117*(C4).

Jones, H., and J. Marshall (1993), Convection with rotation in a neutral ocean: A study of open-ocean deep convection, *Journal of Physical Oceanography*, *23*(6), 1009–1039.

Kalnay, E., M. Kanamitsu, R. Kistler, W. Collins, D. Deaven, L. Gandin, M. Iredell, S. Saha, G. White, J. Woollen, Y. Zhu, A. Leetmaa, R. Reynolds, M. Chelliah, W. Ebisuzaki, W. Higgins, J. Janowiak, K. C. Mo, C. Ropelewski, J. Wang, R. Jenne, and D. Joseph (1996), The ncep/ncar 40-year reanalysis project, *Bulletin of the American Meteorological Society*, *77*(3), 437–471, doi:10.1175/1520-0477(1996)077⟨0437:TNYRP⟩2.0.CO;2.

Katsman, C. A., M. A. Spall, and R. S. Pickart (2004), Boundary current eddies and their role in the restratification of the labrador sea, *Journal of Physical Oceanography*, *34*(9), 1967–1983, doi:10.1175/1520-0485(2004)034⟨1967:bceatr⟩2.0.co;2.

Keeling, R. F. (1993), On the role of large bubbles in air-sea gas exchange and supersaturation in the ocean, *Journal of Marine Research*, *51*(2), 237–271.

Keeling, R. F., and H. E. Garcia (2002), The change in oceanic o-2 inventory associated with recent global warming, *Proceedings of the National Academy of Sciences of the United States of America*, *99*(12), 7848–7853, doi:10.1073/Pnas.122154899.

Keeling, R. F., R. P. Najjar, M. L. Bender, and P. P. Tans (1993), What atmospheric oxygen measurements can tell us about the global carbon-cycle, *Global Biogeochemical Cycles*, *7*(1), 37–67, doi:Doi10.1029/92gb02733.

Keeling, R. F., A. Körtzinger, and N. Gruber (2010), Ocean deoxygenation in a warming world, *Annual Review of Marine Science*, *2*, 199–229, doi:10.1146/Annurev.Marine.010908.163855.

Kihm, C., and A. Körtzinger (2010), Air-sea gas transfer velocity for oxygen derived from float data, *Journal of Geophysical Research: Oceans*, *115*(C12), n/a–n/a, doi:10.1029/2009JC006077, c12003.

Körtzinger, A., J. Schimanski, U. Send, and D. Wallace (2004), The ocean takes a deep breath, *Science*, *306*(5700), 1337–1337, doi:10.1126/science.1102557.

Laffoley, D., and J. Baxter (2019), *Ocean Deoxygenation:Everyone's Problem - Causes, Impacts, Consequences and Solutions*, IUCN.

Large, W. G., J. C. Mcwilliams, and S. C. Doney (1994), Oceanic vertical mixing - a review and a model with a nonlocal boundary-layer parameterization, *Reviews of Geophysics*, *32*(4), 363–403, doi:Doi10.1029/94rg01872.

Laws, E. A., P. G. Falkowski, W. O. Smith, H. Ducklow, and J. J. McCarthy (2000), Temperature effects on export production in the open ocean, *Global Biogeochemical Cycles*, *14*(4), 1231–1246, doi:10.1029/1999gb001229.

Lazier, J. (1980), Oceanographic conditions at ocean weather ship bravo, 1964-1974, *Atmos. Ocean*, *18*, 227–238.

Lazier, J., R. Hendry, A. Clarke, I. Yashayaev, and P. Rhines (2002), Convection and restratification in the labrador sea, 1990-2000, *Deep-Sea Research Part I-Oceanographic Research Papers*, *49*(10), 1819–1835, doi:10.1016/s0967-0637(02)00064-x.

Luo, H., A. Bracco, and E. Di Lorenzo (2011), The interannual variability of the surface eddy kinetic energy in the labrador sea, *Progress in Oceanography*, *91*(3), 295–311, doi:10.1016/j.pocean.2011.01.006.

Luo, H., A. Bracco, and F. Zhang (2014), The seasonality of convective events in the labrador sea, *Journal of Climate*, *27*(17), 6456–6471.

Luo, H., R. M. Castelao, A. K. Rennermalm, M. Tedesco, A. Bracco, P. L. Yager, and T. L. Mote (2016), Oceanic transport of surface meltwater from the southern greenland ice sheet, *Nature Geosci*, *advance online publication*, doi: 10.1038/ngeo2708http://www.nature.com/ngeo/journal/vaop/ncurrent/abs/ngeo2708.html#supplementary-information.

Manning, A., and R. F. Keeling (2006), Global oceanic and land biotic carbon sinks from the scripps atmospheric oxygen flask sampling network, *Tellus B: Chemical and Physical Meteorology*, *58*(2), 95–116.

Marshall, J., and F. Schott (1999), Open-ocean convection: Observations, theory, and models, *Reviews of Geophysics*, *37*(1), 1–64, doi:10.1029/98rg02739.

Marshall, J., C. Hill, L. Perelman, and A. Adcroft (1997a), Hydrostatic, quasi-hydrostatic, and nonhydrostatic ocean modeling, *Journal of Geophysical Research: Oceans*, *102*(C3), 5733–5752.

Marshall, J., A. Adcroft, C. Hill, L. Perelman, and C. Heisey (1997b), A finite-volume, incompressible navier stokes model for studies of the ocean on parallel computers, *Journal of Geophysical Research: Oceans*, *102*(C3), 5753–5766.

Matear, R. J., A. C. Hirst, and B. I. McNeil (2000), Changes in dissolved oxygen in the Southern Ocean with climate change, *Geochem. Geophys. Geosyst.*, *1*, 1050–12, doi: 10.1029/2000GC000086.

Merlivat, L., and L. Memery (1983), Gas exchange across an air-water interface: Experimental results and modeling of bubble contribution to transfer, *Journal of Geophysical Research: Oceans*, *88*(C1), 707–724.

Monahan, E. C. (1993), Occurrence and evolution of acoustically relevant sub-surface bubble plumes and their associated, remotely monitorable, surface whitecaps, in *Natural Physical Sources of Underwater Sound*, pp. 503–517, Springer.

Monahan, E. C., and T. Torgersen (1990), The enhancement of air-sea gas exchange by oceanic whitecapping, in *Air-Water Mass Transfer*, pp. 608–617, ASCE.

Morel, F., and N. Price (2003), The biogeochemical cycles of trace metals in the oceans, *Science*, *300*(5621), 944–947.

Najjar, R. G., and R. F. Keeling (2000), Mean annual cycle of the air-sea oxygen flux: A global view, *Global Biogeochemical Cycles*, *14*(2), 573–584, doi:Doi10.1029/1999gb900086.

Nightingale, P. D., G. Malin, C. S. Law, A. J. Watson, P. S. Liss, M. I. Liddicoat, J. Boutin, and R. C. Upstill-Goddard (2000), In situ evaluation of air-sea gas exchange parameterizations using novel conservative and volatile tracers, *Global Biogeochem. Cycles*, *14*(1), 373–387.

Pham, A. L., and T. Ito (2019), Ligand binding strength explains the distribution of iron in the north atlantic ocean, *Geophysical Research Letters*, *46*(13), 7500–7508.

Pickart, R. S., D. J. Torres, and R. A. Clarke (2002), Hydrography of the labrador sea during active convection, *Journal of Physical Oceanography*, *32*(2), 428–457, doi:10.1175/1520-0485(2002)032⟨0428:hotlsd⟩2.0.co;2.

Plattner, G.-K., F. Joos, and T. F. Stocker (2002), Revision of the global carbon budget due to changing air-sea oxygen fluxes, *Global Biogeochem. Cycles*, *16*, 1096, doi:10.1029/2001GB001746.

Pörtner, H. O., and R. Knust (2007), Climate change affects marine fishes through the oxygen limitation of thermal tolerance, *science*, *315*(5808), 95–97.

Redfield, A. C. (1958), The biological control of chemical factors in the environment, *American scientist*, *46*(3), 230A–221.

Schlesinger, W. H., and E. S. Bernhardt (2013), *Biogeochemistry: an analysis of global change*, Academic press.

Schlitzer, R. (2000a), Electronic atlas of woce hydrographic and tracer data now available, *Eos, Transactions American Geophysical Union*, *81*(5), 45–45.

Schlitzer, R. (2000b), *Applying the adjoint method for biogeochemical modeling: Export of particulate organic matter in the world ocean*, *Geophysical Monograph Series*, vol. 114, pp. 107–124.

Schmidtko, S., L. Stramma, and M. Visbeck (2017), Decline in global oceanic oxygen content during the past five decades, *Nature*, *542*(7641), 335–339.

Schudlich, R., and S. Emerson (1996), Gas supersaturation in the surface ocean: The roles of heat flux, gas exchange, and bubbles, *Deep Sea Research Part II: Topical Studies in Oceanography*, *43*(2), 569–589.

Siegel, D. A., K. O. Buesseler, S. C. Doney, S. Sailley, M. J. Behrenfeld, and P. W. Boyd (2014), Global assessment of ocean carbon export using food-web models and satellite observations, *Global Biogeochemical Cycles*, *28*, doi:10.1002/2013GB004743.

Sun, D., T. Ito, and A. Bracco (2017), Oceanic uptake of oxygen during deep convection events through diffusive and bubble-mediated gas exchange, *Global Biogeochemical Cycles*, *31*(10), 1579–1591.

Tagklis, F., T. Ito, and A. Bracco (2020), Modulation of the north atlantic deoxygenation by the slowdown of the nutrient stream, *Biogeosciences Discussions*, pp. 1–22.

Talley, L. D. (2011), *Descriptive physical oceanography: an introduction*, Academic press.

Talley, L. D., and M. S. McCartney (1982), Distribution and circulation of labrador sea water, *Journal of Physical Oceanography*, *12*(11), 1189–1205, doi:10.1175/1520-0485(1982)012⟨1189:dacols⟩2.0.co;2.

van Aken, H. M., M. F. de Jong, and I. Yashayaev (2011), Decadal and multi-decadal variability of labrador sea water in the north-western north atlantic ocean derived from tracer distributions: Heat budget, ventilation, and advection, *Deep-Sea Research Part I-Oceanographic Research Papers*, *58*(5), 505–523, doi:10.1016/j.dsr.2011.02.008.

Vaquer-Sunyer, R., and C. M. Duarte (2008), Thresholds of hypoxia for marine biodiversity, *Proceedings of the National Academy of Sciences*, *105*(40), 15,452–15,457, doi:10.1073/pnas.0803833105.

Wanninkhof, R. (1992), Relationship between wind speed and gas exchange over the ocean, *Journal of Geophysical Research: Oceans*, *97*(C5), 7373–7382, doi:10.1029/92JC00188.

Williams, R. G., and M. J. Follows (2011), *Ocean dynamics and the carbon cycle: Principles and mechanisms*, Cambridge University Press.

Woolf, D. K., and S. Thorpe (1991), Bubbles and the air-sea exchange of gases in near-saturation conditions, *Journal of marine research*, *49*(3), 435–466.

Yashayaev, I. (2007), Hydrographic changes in the labrador sea, 1960-2005, *Progress in Oceanography*, *73*(3), 242–276, doi:10.1016/j.pocean.2007.04.015.

Yashayaev, I., and J. W. Loder (2016), Recurrent replenishment of labrador sea water and associated decadal-scale variability, *Journal of Geophysical Research: Oceans*, *121*(11), 8095–8114, doi:10.1002/2016JC012046.

Yashayaev, I., M. Bersch, and H. M. van Aken (2007), Spreading of the labrador sea water to the irminger and iceland basins, *Geophysical Research Letters*, *34*(10), doi:10.1029/2006gl028999.